LIBRARY
TECHNICAL REPORT SECTION
NAVAL POSTGRADUATE SCHOOL
MONTEREY, CALIFORNIA 93940

NPS63-80-003

NAVAL POSTGRADUATE SCHOOL

Monterey, California

AN EMBEDDED MIXED LAYER-OCEAN CIRCULATION MODEL

David Adamec, Russell L. Elsberry,
Roland W. Garwood, Jr. and Robert L. Haney

December 1980

Approved for public release; distribution unlimited.

Prepared for: Chief of Naval Research (Code 481)
NSTL Station, MS 39529

FEDDOCS
D 208.14/2:NPS-63-80-003

DUDLEY KNOX LIBRARY
NAVAL POSTGRADUATE SCHOOL
MONTEREY, CA 93943-5101

NAVAL POSTGRADUATE SCHOOL
Monterey, California 93940

Rear Admiral John J. Ekelund
Superintendent

D. A. Schrady
Acting Provost

The work reported herein was initially supported by the Naval Postgraduate School Foundation Research Program with funds provided by the Chief of Naval Research. Subsequent support was provided by the Office of Naval Research, Ocean Science and Technology Branch, through grants to R. Elsberry and R. Garwood, and to R. Haney.

This report was prepared by:

SECURITY CLASSIFICATION OF THIS PAGE (When Data Entered)

REPORT DOCUMENTATION PAGE

READ INSTRUCTIONS BEFORE COMPLETING FORM

1. REPORT NUMBER: NPS63-80-003	2. GOVT ACCESSION NO.
3. RECIPIENT'S CATALOG NUMBER	
4. TITLE (and Subtitle): An Embedded Mixed Layer-Ocean Circulation Model	5. TYPE OF REPORT & PERIOD COVERED: Report for October 1977 - September 1980
	6. PERFORMING ORG. REPORT NUMBER
7. AUTHOR(s): D. Adamec, R. Elsberry, R. Garwood, Jr. and R. Haney	8. CONTRACT OR GRANT NUMBER(s): NR083-275-5 and NR083-275-6
9. PERFORMING ORGANIZATION NAME AND ADDRESS: Naval Postgraduate School, Monterey, California 93940	10. PROGRAM ELEMENT, PROJECT, TASK AREA & WORK UNIT NUMBERS: 61153N
11. CONTROLLING OFFICE NAME AND ADDRESS: Office of Naval Research, Code 480, NSTL Station, MS 39529	12. REPORT DATE: December 1980
	13. NUMBER OF PAGES: 66
14. MONITORING AGENCY NAME & ADDRESS (if different from Controlling Office)	15. SECURITY CLASS. (of this report): Unclassified
	15a. DECLASSIFICATION/DOWNGRADING SCHEDULE

16. DISTRIBUTION STATEMENT (of this Report)

Approved for public release; distribution unlimited.

17. DISTRIBUTION STATEMENT (of the abstract entered in Block 20, if different from Report)

18. SUPPLEMENTARY NOTES

Submitted for publication in Dynamics of Atmospheres and Oceans.

19. KEY WORDS (Continue on reverse side if necessary and identify by block number)

Ocean circulation model
Ocean mixed-layer model
Oceanic mixing and advection

20. ABSTRACT (Continue on reverse side if necessary and identify by block number)

The rationale and numerical technique of embedding an oceanic bulk mixed layer model with a multi-level primitive equation model is presented. In addition to the usual prognostic variables that exist in a multi-level primitive equation model, the embedded model predicts the depth of the well mixed layer as well as the jumps in temperature and velocity that occur at the base of that layer. The depth of the mixed layer need not coincide with any of the fixed model levels used in the primitive equations calculations.

DD FORM 1 JAN 73 1473 EDITION OF 1 NOV 65 IS OBSOLETE
S/N 0102-014-6601

SECURITY CLASSIFICATION OF THIS PAGE (When Data Entered)

In addition to advective changes, the mixed layer can deepen by entrainment and it can reform at a shallower depth in the absence of entrainment. When the mixed layer reforms at a shallower depth, the vertical profile of temperature below the new, shallower mixed layer is adjusted to fit the fixed-level structure used in the primitive equations calculations using a method which conserves heat, momentum and potential energy. Finally, a dynamic stability condition, which includes a consideration of both the vertical current shear and the vertical temperature gradient, is introduced in place of the traditional "convective adjustment".

A two-dimensional version of the model is used to test the embedded model formulations and to study the response of the ocean to a stationary axisymmetric hurricane. The model results indicate a strong interdependence between vertical turbulent mixing and advection of heat.

GRADLEY KNOX LIBRARY
NAVAL POSTGRADUATE SCHOOL
MONTEREY, CA 93943-5101

AN EMBEDDED MIXED LAYER-OCEAN CIRCULATION MODEL

David Adamec[1], Russell L. Elsberry[1],
Roland W. Garwood, Jr.[2] and Robert L. Haney[1]

Naval Postgraduate School, Monterey, CA 93940 (U.S.A.)

[1]Department of Meteorology

[2]Department of Oceanography

ABSTRACT

The rationale and numerical technique of embedding an oceanic bulk mixed layer model with a multi-level primitive equation model is presented. In addition to the usual prognostic variables that exist in a multi-level primitive equation model, the embedded model predicts the depth of the well mixed layer as well as the jumps in temperature and velocity that occur at the base of that layer. The depth of the mixed layer need not coincide with any of the fixed model levels used in the primitive equations calculations.

In addition to advective changes, the mixed layer can deepen by entrainment and it can reform at a shallower depth in the absence of entrainment. When the mixed layer reforms at a shallower depth, the vertical profile of temperature below the new, shallower mixed layer is adjusted to fit the fixed-level structure used in the primitive equations calculations using a method which conserves heat, momentum and potential energy. Finally, a dynamic stability condition, which includes a consideration of both the vertical current shear and the vertical temperature gradient, is introduced in place of the traditional "convective adjustment".

A two-dimensional version of the model is used to test the embedded model formulations and to study the response of the ocean to a stationary axisymmetric hurricane. The model results indicate a strong interdependence between vertical turbulent mixing and advection of heat.

1. INTRODUCTION

The value of numerical models for the study of ocean dynamics has become widely recognized in recent years (National Academy of Sciences, 1975; Kraus, 1977; WMO/ICSU, 1977). However, no single model has been developed that can resolve the full range of space and time scales commonly observed in the ocean. Thus, the characteristics of each numerical model differ considerably and they are usually tailored to the space and time scales of the oceanic phenomena being studied. The time scales to which various models have been applied range from decades for the deep ocean circulation to seasonal, synoptic and diurnal for near-surface phenomena.

Numerical models of the ocean can be separated into two broad categories. These are the basin-wide or global ocean models which attempt to simulate the ocean circulation on seasonal or longer time scales, and the one-dimensional models which attempt to simulate the locally forced response at seasonal or shorter time scales. The former type of model is referred to as an ocean general circulation model (OGCM) and the latter type, which usually focuses on vertical mixing processes, is referred to as a mixed layer model (MLM). The most recent comprehensive reviews of OGCM's and MLM's are those by Holland (1979), Robinson, Harrison and Haidvogel (1979), Bryan (1979), Haney (1979) and Garwood (1979).

The present study, which addresses the problem of embedding a one-dimensional mixed layer model into a numerical model of the general circulation, was motivated by several factors. First, the solution of this problem was recently set as an important goal by an international group of scientists studying ocean models and

their relation to climate (WMO/ICSU, 1977). In addition, there are a wide variety of important ocean problems involving intermediate and mesoscale motions which could be addressed with a realistically embedded mixed-layer ocean circulation model. These problems include studies of open ocean fronts, coastal and equatorial upwelling and the ocean's response to intense atmospheric storms. It is also anticipated that an embedded mixed layer ocean-circulation model will eventually have a number of important applications in the problem of operational ocean prediction.

In this paper, the rationale and numerical technique of embedding a model of the mixed layer into an ocean circulation model is presented. The resulting embedded model has been tested in a variety of ocean studies. The simulation of the ocean's response to hurricane forcing is presented here because the large horizontal variations in advection and mixing in such a case (Madala and Piacsek, 1977) provide a severe test of the embedded model. Model simulations of the oceanic response to less extreme forcing, which illustrate more subtle aspects of the embedding, will be published later. Our purpose is not to intercompare possible mixing parameterizations, but rather to describe the embedding of a particular bulk mixed layer model within a multi-level ocean circulation model.

2. MODEL EQUATIONS AND BOUNDARY CONDITIONS

In this section, the equations and boundary conditions for the embedded mixed-layer ocean circulation model, as applied to the hurricane forcing problem, are presented. Details of the numerical formulation, however, are given in the Appendix.

The ocean is taken to be hydrostatic and incompressible and the density is a linear function of temperature alone. For computational economy and because hurricane forcing is nearly axisymmetric, the ocean's response is assumed to be axisymmetric. In addition, the Coriolis parameter is assumed to be constant. The governing equations are written in radial coordinates as

$$\frac{\partial u}{\partial t} = -\frac{1}{r}\frac{\partial}{\partial r}(uru) - \frac{\partial}{\partial z}(wu) + (f + \frac{v}{r})v - \frac{\partial}{\partial r}(\frac{p}{\rho_o}) + \frac{1}{r}\frac{\partial}{\partial r}(rA_M\frac{\partial u}{\partial r}) - \frac{\partial}{\partial z}(\overline{w'u'}) \tag{2.1}$$

$$\frac{\partial v}{\partial t} = -\frac{1}{r}\frac{\partial}{\partial r}(urv) - \frac{\partial}{\partial z}(wv) - (f + \frac{v}{r})u + \frac{1}{r}\frac{\partial}{\partial r}(rA_M\frac{\partial v}{\partial r}) - \frac{\partial}{\partial z}(\overline{w'v'}) \tag{2.2}$$

$$\frac{\partial T}{\partial t} = -\frac{1}{r}\frac{\partial}{\partial r}(urT) - \frac{\partial}{\partial z}(wT) + \frac{1}{r}\frac{\partial}{\partial r}(rA_T\frac{\partial T}{\partial r}) - \frac{\partial}{\partial z}(\overline{w'T'}) \tag{2.3}$$

$$\frac{1}{r}\frac{\partial}{\partial r}(ur) + \frac{\partial w}{\partial z} = 0 \tag{2.4}$$

$$\frac{\partial p}{\partial z} = -\rho g \tag{2.5}$$

$$\rho = \rho_o(1 - \alpha(T-T_o)) \tag{2.6}$$

where u, v and w are the radial, tangential and vertical components of velocity, respectively; p is pressure; T is temperature; ρ is density; A_M and A_T are coefficients of horizontal eddy viscosity and conductivity, respectively; α is the coefficient of

thermal expansion; and ρ_o is the density of water at the reference temperature, T_o. The values of constants used in the hurricane forcing experiments are given in Table 1. The terms $(\overline{w'u'})$, $(\overline{w'v'})$ and $(\overline{w'T'})$ represent ensemble average turbulent fluxes and are described below. In (2.1)-(2.3), the advection terms have been written in flux form using the continuity equation (2.4).

The above model equations are applied to an oceanic region extending from the surface to a depth of H = 964 m and from the storm center (r = 0) to a radial distance of R = 450 km. There are no fluxes of mass, momentum or heat across the boundaries except at the surface where a steady wind stress and upward heat flux are prescribed. The specific conditions are

$$u = A_M \frac{\partial u}{\partial r} = A_M \frac{\partial v}{\partial r} = A_T \frac{\partial T}{\partial r} = 0; \quad r=0,R \tag{2.7}$$

$$w=0; \quad z=0,-H \tag{2.8}$$

and

$$\left.\begin{aligned} -(\overline{w'T'}) &= Q(r)/\rho_o C \\ -(\overline{w'u'}) &= \tau_r(r)/\rho_o \\ -(\overline{w'v'}) &= \tau_\theta(r)/\rho_o \end{aligned}\right\} \quad ; \quad z=0 \tag{2.9}$$

$$(\overline{w'T'}) = (\overline{w'u'}) = (\overline{w'v'}) = 0; \quad z=-H. \tag{2.10}$$

The forcing functions Q, τ_r and τ_θ are shown in Fig. 1. The stress is calculated from a prescribed wind, the magnitude of which increases linearly with r from the eye wall of the storm (r = 4.5 km) to the radius of maximum winds (r = 45 km); decreases like $r^{-1/2}$ from there to 360 km; and then decreases linearly to zero at the boundary (450 km). This wind profile results in the wind stress components shown in Fig. 1 and a curl, $\partial(\tau_\theta r)/r\partial r$, which is zero inside the eye of the storm; positive and increasing linearly from r = 4.5 km to 45 km; zero from 45 km to 360 km and negative from r = 360 km to the boundary. The maximum tangential stress of nearly 36 dPa corresponds to a maximum surface wind speed of 50 m s^{-1}. The small inward radial stress component, $\tau_r < 0$, results from a cross isobaric surface inflow angle of 20 degrees. The effect of other choices of wind stress profiles will be reported elsewhere.

Putting w = 0 at the top of the ocean, as in (2.8), is known as the rigid-lid approximation and it requires the divergence of the vertically averaged motion to be zero. In the present model, we simplify the dynamics even further by assuming that the vertically averaged motion itself is zero. This simplification is justified in the present case because the shear currents spun up by the surface stress are much greater than the dynamically induced barotropic currents. Subtracting the vertical average of (2.1) and (2.2) from (2.1) and (2.2) respectively gives the prediction equations for the vertical shear currents

$$\frac{\partial u}{\partial t} = -\frac{1}{r}\frac{\partial}{\partial r}(uru) - \frac{\partial}{\partial z}(wu) + (f + \frac{v}{r})v$$

$$-\frac{\partial}{\partial r}(\frac{\hat{p}}{\rho_o}) + \frac{1}{r}\frac{\partial}{\partial r}(rA_M\frac{\partial u}{\partial r}) - \frac{\partial}{\partial z}(\overline{w'u'})$$

$$-[-\frac{1}{r}\frac{\partial}{\partial r}(\widetilde{uru}) + \frac{\widetilde{vv}}{r} + \frac{\tau_r}{\rho_o H}] \qquad (2.11)$$

$$\frac{\partial v}{\partial t} = -\frac{1}{r}\frac{\partial}{\partial r}(urv) - \frac{\partial}{\partial z}(wv) - (f + \frac{v}{r})u$$

$$+\frac{1}{r}\frac{\partial}{\partial r}(rA_M\frac{\partial v}{\partial r}) - \frac{\partial}{\partial z}(\overline{w'v'})$$

$$-[-\frac{1}{r}\frac{\partial}{\partial r}(\widetilde{urv}) - \frac{\widetilde{vu}}{r} + \frac{\tau_\theta}{\rho_o H}] \ , \qquad (2.12)$$

where $\widetilde{(\ )}$ denotes a vertical average over the total ocean depth H, $\hat{p}$ is $p-\tilde{p}$, and (u,v) are now the shear currents having zero vertical average. By integrating (2.5) and using (2.6), $\hat{p}$ is obtained as a function of T alone, thus

$$\hat{p} = \int_z^o \rho_o(1-\alpha(T-T_o))gd\lambda - \frac{1}{H}\int_{-H}^{o}[\int_z^o \rho_o(1-\alpha(T-T_o))gd\lambda]dz \ . \qquad (2.13)$$

The turbulence closure method described below requires a prognostic equation for the depth of the well-mixed layer, denoted by h. This equation is derived by integrating the continuity equation (2.4) over the mixed layer, and applying the boundary condition $w = 0$ at $z = 0$. Thus,

$$\frac{1}{r}\int_{-h}^{o}\frac{\partial}{\partial r}(ur)\,dz \quad -w_{-h} = 0 ,$$

or

$$\frac{1}{r}\left[\frac{\partial}{\partial r}\int_{-h}^{o} rudz - ru_{-h}\frac{\partial h}{\partial r}\right] - w_{-h} = 0 . \tag{2.14}$$

Denoting an average over h by $\langle(\,)\rangle \equiv \frac{1}{h}\int_{-h}^{o}(\,)\,dz$ and noting that

$$\frac{dh}{dt} = \frac{\partial h}{\partial t} + u_{-h}\frac{\partial h}{\partial r} ,$$

(2.14) reduces to

$$\frac{\partial h}{\partial t} + \frac{1}{r}\frac{\partial}{\partial r}(rh\langle u\rangle) = \frac{dh}{dt} + w_{-h} \equiv w_e . \tag{2.15}$$

The right hand side of (2.15), denoted w_e, is an entrainment velocity which is related to the net acquisition of mass in the mixed layer. Its parameterization is described below. The six equations (2.11), (2.12), (2.3), (2.13), (2.4) and (2.15), along with the boundary conditions (2.7)-(2.10) represent a closed system of equations for the six dependent variables u,v,T,$\hat{p}$,w and h provided the turbulence quantities, $(\overline{w'u'})$, w_e etc., are parameterized. The values of the turbulent fluxes of heat and momentum

at the top and bottom of the model ocean are given by the boundary conditions (2.9) and (2.10). The parameterization of the turbulent fluxes within the water column is given in the following sections.

3. VERTICAL DIFFUSION

The classical solution to the problem of parameterizing the vertical turbulent fluxes of heat and momentum is the posing of eddy viscosity and eddy conductivity formulations such that

$$\left.\begin{aligned} \overline{w'u'} &= -K_M \frac{\partial u}{\partial z} \\ \overline{w'v'} &= -K_M \frac{\partial v}{\partial z} \\ \overline{w'T'} &= -K_T \frac{\partial T}{\partial z} \end{aligned}\right\} . \qquad (3.1)$$

This is reasonable if gradient diffusion is physically plausible, and if the values of K_M and K_T are known to be approximately constant. This approximation has been shown to produce realistic vertical profiles of temperature in the upper ocean below the depth of immediate influence of the stirring action of the atmospheric forcing. Therefore, this parameterization is employed at all depths below the ocean surface mixed layer, with K_M and K_T both equal to 0.5 cm s^{-1}. It is possible that the dynamic instability parameterization described later could alone provide the desired mixing below the turbulent boundary layer.

The above parameterization of the vertical fluxes is not satisfactory, however, between the ocean surface and the top of the stable thermocline. In this region of intense turbulent mixing, the appropriate values of K_M and K_T would be two to three orders of magnitude larger and time dependent. Even if realistic values

of K_M and K_T can be computed from scaling arguments or from more sophisticated turbulence closure assumptions, the most important problem is to determine the depth below which the intensity of the turbulence becomes insignificant. The position of this discontinuity is at z = -h, the depth of the bottom of the ocean surface turbulent boundary layer or mixed layer. Thus an entrainment model is needed to compute h(r,t).

4. ENTRAINMENT AND MIXED LAYER MODEL FORMULATION

In the Garwood (1977) model, the buoyancy flux at the base of the turbulent boundary layer is modeled according to

$$\alpha g \, (\overline{w'T'})_{-h} = - \langle \overline{w'w'} \rangle^{1/2} \langle \bar{E} \rangle / h \, . \tag{4.1}$$

This expression is derived from the local (z = -h) turbulent kinetic energy budget. In the entrainment zone, the buoyant damping attributable to $(\overline{w'T'})_{-h}$ is assumed to be balanced by the convergence of turbulent kinetic energy flux. This convergence term is modeled as a function of the turbulent kinetic energy components and the vertical distance over which this energy must be transported. Here $\langle \overline{w'w'} \rangle$, and $\langle \bar{E} \rangle$ are the bulk (mixed layer average) values of the vertical component and total turbulent kinetic energies respectively. The prognostic equations for these mixed layer turbulence variables are derived using the bulk second order closure methods of Garwood (1977) and are

$$\frac{\partial}{\partial t} (h\langle \bar{E} \rangle/2) = m u_*^3 - \alpha g h \, (\overline{w'T'})_{-h}/(2Ri^*) - (\langle \bar{E} \rangle^{1/2} + fh) \langle \bar{E} \rangle \tag{4.2}$$

$$\frac{\partial}{\partial t}\left(h\langle\overline{w'w'}\rangle/2\right) = \alpha g h\left(\left(\overline{w'T'}\right)_{-h} - \left(\overline{w'T'}\right)_{o}\right)/2$$

$$+ \left(\langle\bar{E}\rangle - 3\langle\overline{w'w'}\rangle\right)\langle\bar{E}\rangle^{1/2} - \left(\langle\bar{E}\rangle^{1/2} + fh\right)\langle\bar{E}\rangle/3 \ , \qquad (4.3)$$

In (4.2) and (4.3), $u_* = (\tau/\rho_a)^{1/2}$ with τ the magnitude of the surface stress and ρ_a the (constant) air density, and $Ri^* = \alpha g h \Delta T / (\Delta u^2 + \Delta v^2)$ is the bulk Richardson number. The quantities ΔT, Δu and Δv are the temperature and velocity jumps, or differences, between the values in the mixed layer (assumed to be vertically uniform) and the underlying stable water. These bulk turbulent kinetic energy equations are solved algebraically by assuming a quasi-steady state for the turbulent kinetic energy budgets:

$$\frac{\partial}{\partial t}\left(h\,\langle\bar{E}\rangle\right) \simeq 0 \ ; \quad \frac{\partial}{\partial t}\left(h\,\langle\overline{w'w'}\rangle\right) \simeq 0 \ .$$

This assumption causes the computed values of $\langle\overline{w'w'}\rangle$ and $\langle E\rangle$ to be in phase with the surface boundary conditions--the wind stress, $\rho_a u_*^2$, and the effective surface buoyancy flux, $\alpha g\left(\overline{w'T'}\right)_o$. In a study of nonstationarity including a diurnal cycle (Garwood and Yun, 1979), this approximation was found to be sufficiently accurate for time scales greater than a few hours. The motivation for this quasi-steady state assumption is a substantial gain in numerical efficiency. The time step is limited more by the requirement of resolving the diurnal forcing than for accuracy in solving the turbulent kinetic energy equation. This assumption also makes the

boundary layer model more compatible with the numerical requirements of the ocean circulation model.

For some applications, the bulk Richardson number term in (4.2) may also be neglected if $Ri^* >> 1$. However, this term should be retained in situations in which strong shears might be expected across the entrainment zone. Niiler (1975) and DeSzoeke and Rhines (1976) demonstrate that this term may be significant at the outset of a deepening event, provided the initial mixed layer depth is small.

Once the entrainment buoyancy flux is known from (4.1), the downward fluxes of momentum associated with entrainment at the base of the mixed layer, $(\overline{w'u'})_{-h}$ and $(\overline{w'v'})_{-h}$, are given by

$$- (\overline{w'u'})_{-h} = w_e \Delta u = - (\overline{w'T'})_{-h} \frac{\Delta u}{\Delta T} \qquad (4.1a)$$

$$- (\overline{w'v'})_{-h} = w_e \Delta v = - (\overline{w'T'})_{-h} \frac{\Delta v}{\Delta T} , \qquad (4.1b)$$

where the entrainment velocity,

$$w_e = - \frac{(\overline{w'T'})_{-h}}{\Delta T} . \qquad (4.1c)$$

The above mixed layer formulation was selected for coupling with an ocean circulation model because of its general applicability and because it has been extensively tested and calibrated at several weather ship stations (Garwood and Adamec, 1980). The general applicability of the above model is attributed to two

important features: (1) An annual-period cyclical steady state is possible because of a dissipative limitation to deepening that is dependent upon planetary rotation; (2) Entrainment flux is a function of implicitly computed values of both horizontal and vertical components of turbulent kinetic energy. As a result, the fraction of turbulent kinetic energy that is available for mixing at the base of the mixed layer is not a constant but is dependent upon both the surface buoyancy flux and the surface friction velocity. These desirable properties are obtained using second order closure techniques without sacrificing the bulk model's numerical efficiency which is necessary for practical application of the final coupled system with large two and three dimensional arrays.

Boundary layer deepening by entrainment

The entrainment heat flux, $(\overline{w'T'})_{-h}$, is determined algebraically from (4.1), and the steady state forms of (4.2) and (4.3) using given values of u_*, $(\overline{w'T'})_o$, h and Ri^*. This heat flux is then imposed upon the given temperature profile. The new h and the new momentum and temperature profiles are unique solutions provided: (i) the mixed layer ($0 > z > -h$) is homogeneous; (ii) the value of h is made just large enough to prevent unstable density profiles ($\partial T/\partial z > 0$); and (iii) heat is conserved. Note that the depth of the bottom of the mixed layer is not forced to coincide with any of the prescribed model levels or interfaces between levels. As a result, there is added vertical resolution in the vicinity of the mixed layer interface. This extra resolution is very desirable because the vertical structure of the thermocline determines the potential energy of the upper ocean which is

important for both the dynamics of the boundary layer and the larger scale baroclinic circulation.

Boundary layer shallowing

Equally important in a mixed layer model of general applicability is the prediction of boundary layer shallowing. This phenomenon occurs when there is inadequate vertical turbulent energy to transport heat down to the base of the existing mixed layer. The (new) depth at which the vertical flux ($\overline{w'T'}$) vanishes establishes the bottom of the turbulent boundary layer and what will be the base of the new mixed layer. In the present model, this occurs when $\langle\overline{w'w'}\rangle$ approaches zero. Then (4.1) no longer applies and the steady state forms of (4.2) and (4.3) reduce to the following diagnostic equations for the new mixed layer depth

$$0 = mu_*^3 - (\langle\bar{E}\rangle^{1/2} + fh)\langle\bar{E}\rangle \tag{4.2a}$$

$$0 = -\alpha gh(\overline{w'T'})_o/2 + \langle\bar{E}\rangle^{3/2} - (\langle\bar{E}\rangle^{1/2} + fh)\langle\bar{E}\rangle/3 \ . \tag{4.3a}$$

Without the term involving the planetary rotation, or if the downward surface buoyancy flux is dominant, h is proportional to the Obukhov length scale, $L = u_*^3/(\alpha g(\overline{w'T'})_o)$. On the other hand, if $(\overline{w'T'})_o = 0$, h is proportional to u_*/f. In general, however, the depth of the shallowing mixed layer is a function of the two non-dimensional parameters, h/L and hf/u_*.

In a numerical model, the formation of a new, shallower mixed layer is potentially a problem because the interfacial structure of previously created mixed layers can not be exactly preserved

with a relatively coarse vertical grid. In the present model, this potential problem is avoided using a numerical procedure (see Appendix) that conserves heat, momentum and potential energy, while minimizing changes in the vertical density structure. Although potential energy is conserved during the shallowing process, no attempt is made to exactly conserve mean kinetic energy.

5. DYNAMIC STABILITY CONDITION

In the derivation of the above bulk mixed layer model, it is assumed that the turbulent boundary layer is dynamically unstable and that the underlying water column is dynamically stable as measured by the gradient Richardson number, Ri. In the entrainment zone ($-h \leq z \leq -h-d$), dynamic stability is assumed to be near neutral; that is $Ri = Ri_{CR} \approx 1/4$. This condition is insufficient in itself to determine the entrainment fluxes or the rate of mixed layer deepening; however, it does lead to a measure of the thickness of the zone: $d \approx Ri_{CR} (\Delta u^2 + \Delta v^2) \alpha g \Delta T$. Deepening of the mixed layer depends upon the added intermittent vertical flux of turbulent kinetic energy from above.

As mentioned earlier, dynamic instability can sometimes occur below the mixed layer, and this will enhance the vertical transport of both heat and momentum. Therefore, in the present model, dynamic stability is enforced throughout the water column by imposing those vertical fluxes of heat and momentum between model levels which are necessary to prevent the gradient Richardson number from going below the critical value, i.e. $Ri(z) \geq Ri_{CR}$. This "dynamical adjustment" is a simple generalization of the "convective adjustment" parameterization which is commonly used in most

ocean general circulation models. Details are given in the Appendix.

It should be pointed out here that the above dynamical stability condition is different from that of Pollard, et al. (1973) and Thompson (1976). In that model, deepening is dependent upon stability as determined by the bulk Richardson number, Ri^*. This is equivalent to the present requirement that there be a constant gradient Richardson number in the entrainment zone only if the thickness of the entrainment zone divided by the mixed layer depth, i.e. d/h, is a constant. There is no physical justification for such an assumption.

6. METHOD OF EMBEDDING

The system of equations for the embedded model includes a prognostic determination of the mixed layer depth. The mixed layer is defined here as being the upper layer of the ocean where turbulent mixing is dominant. The temperature and horizontal velocities are required to be independent of depth in this region.

One of the more important parameters in predicting the evolution of the mixed layer is the dynamic stability at its base. Since density is assumed to be a function of temperature alone, the temperature jump at the base of the mixed layer is critical. The dynamic portion of the model is a level model that predicts the average of a quantity between two specified depths. The base of the mixed layer, however, will rarely lie exactly on a model level. Requiring a sufficiently fine vertical resolution to prevent errors in the thermal and potential energy balances due to the truncation of the mixed layer depth to a model level is

unreasonable both in terms of computer storage and computational time. The problem addressed here is to provide for a meaningful communication between the fixed-level, dynamical part of the model, and the mixed layer part of the model.

The coupling of the dynamical and mixing processes in the model may be considered in two stages. First, the changes in the upper ocean due to advective and diffusive processes are calculated in the dynamical part of the model and put into appropriate form for the mixed layer model. Second, the changes due to surface fluxes and entrainment mixing are calculated in the mixing part of the model and transmitted to the dynamical part of the model. In both of these stages, a special treatment is required for the model level which contains the base of the mixed layer.

At the start of a given timestep, changes due to advective and diffusive processes (including the dynamic adjustment described in Section 5) are calculated for all the GCM layers in the dynamical part of the model and the prognostic variables (u,v,T and h) are stepped forward in time (see the Appendix for details of the time differencing scheme). The special treatment for the layer containing the new mixed layer depth is now described with the aid of Fig. 2 in which the dashed line is the vertical structure used by the dynamical part of the model and the solid line is the vertical structure used by the mixing part of the model. Both the dynamical and the mixing part of the model use the same structure at all levels which lie entirely within the mixed layer. The variable ξ represents u, v, or T. If the base of the mixed layer lies within the k th model level, the value of ξ in the mixed layer portion is

denoted by ξ_1; the value just below the mixed layer is denoted by ξ_2; the integrated average over the model level is denoted by $\bar{\xi}$; while the mixed layer depth is denoted by h. The change $\delta\xi_1$ due to advective and diffusive processes is assigned the value calculated for the GCM layer immediately above (i.e. the layer bounded by $Z_{k-1/2}$ and $Z_{k-3/2}$ in Fig. 2). The base of the mixed layer is constrained to always lie at or below the base of the first model level. The associated change $\delta\xi_2$ is then calculated from the requirement that the weighted average of $\delta\xi_1$ and $\delta\xi_2$ be equal to the change $\delta\bar{\xi}$ predicted for the layer by the dynamical part of the model. Thus,

$$\Delta Z_k \, \delta\bar{\xi} = Z_1 \, \delta\xi_1 + Z_2 \, \delta\xi_2 \, , \qquad (5.1)$$

where Z_1 is the portion of the layer above the new mixed layer and $Z_1 + Z_2 = \Delta Z_k$. In the circulation model, the advective and diffusive changes are based on the average properties in each layer. However, there can be a large velocity and temperature jump across the interface h. The use of a layer mean advecting velocity and layer mean temperature in the dynamical part of the model necessarily introduces an error in the calculation of the change $\delta\bar{\xi}$, which, by our formulation, is introduced into the change assigned to $\delta\xi_2$. The error in $\delta\bar{\xi}$ will be smallest when the depth h is close to one of the interfaces between GCM layers, and it will be largest when h is near the center of a GCM layer. An analogous but slightly more complex formulation is used whenever the dynamically predicted δh causes the base of the mixed layer to move

into an adjacent model layer. Before proceeding to the mixing portion of the timestep, the values of ξ throughout the mixed layer (including ξ_1) are replaced by the vertical average of ξ over the new mixed layer depth. In the particular hurricane simulation shown below, the small amount of turbulent kinetic energy that would be expended (or released) in performing this vertical mixing has been neglected in the turbulent kinetic energy balance. This is clearly justified in the present case since the amount of turbulent kinetic energy generated by shear stress production is so large.

The second stage of the coupling is the mixing portion of the timestep. During this stage, the case with entrainment mixing occurring in association with mixed layer deepening must be distinguished from the case in which the layer reforms at a shallower depth. Consider first the entrainment mode in which the mixed layer model (Section 4) predicts an entrainment heat flux, $(\overline{w'T'})_{-h} < 0$. The mixed layer deepening, $\delta h > 0$, during the timestep Δt is calculated from (4.1c). In this case, a volume of water (per unit area) equal to δh and having property ξ_2 is entrained into the mixed layer having volume (per unit area) equal to h and property ξ_1. This results in a new mixed layer of depth $h + \delta h$ and property $\xi_1 + \delta\xi_1$, where

$$\delta\xi_1 = -\frac{(\xi_1 - \xi_2)\,\delta h}{h + \delta h} \quad . \tag{6.2}$$

Entrainment mixing produces no change in ξ below the new mixed layer depth. If $\xi_1 \geq \xi_2$, which is always true for the temperature

in the model, then $\delta\xi_1 \leq 0$. If the entrainment deepening does not cause the base of the mixed layer to move into an adjacent model layer, then the magnitude of the property jump across the mixed layer, $|\xi_1 - \xi_2|$, will be decreased. In the numerical model, a separate array of ξ_2 values must be stored to permit the jump values, $\xi_1 - \xi_2$, to be always specified for the mixing process. This value, and the mixed layer depth h are the only additional variables which must be retained in coupling the mixing model and the dynamical model (see Appendix for details).

Consider now the case of mixed layer shallowing. In this case the diagnostic relations (4.2a) and (4.3a) are solved for the new mixed layer depth. The heat and momentum fluxed across the surface during the timestep are distributed over the new, shallower depth to produce a new value of ξ_1. A new ξ_2 value is determined from the prior ξ_1. The next advective timestep operates with the new, shallower mixed layer. Some information is lost regarding the deeper structure because provision is made for but one active mixed layer. To preserve some of the information regarding the density jump at the base of a prior mixed layer, the vertical density profile is adjusted to conserve both heat and potential energy whenever the mixed layer reforms at a shallower depth (see Appendix for details).

7. APPLICATION WITH STATIONARY HURRICANE FORCING

The purpose of this section is to demonstrate the capability of the embedded mixed layer-ocean circulation model to simulate realistic upper ocean changes in response to hurricane forcing. Such strong forcing as that of a hurricane is used because a large

horizontal gradient in the advective and mixing response is expected and this will provide an extreme test of the model. No attempt is made to compare the results of the present embedded model to the results of other models utilizing different mixing parameterizations. Such a comparison is beyond the scope of the present paper.

The classical model simulation of the ocean's response to hurricane forcing is that of O'Brien and Reid (1967) using an axisymmetric, one-layer model. The extension of this type of model to two horizontal dimensions is given by Chang and Anthes (1978), while the response of a multi-level circulation model is described by Madala and Piacsek (1977). As a result of these and other studies, certain features of the dynamical response of the ocean to a stationary hurricane are well known. The currents in the upper layers of the ocean tend to circulate in the same sense as the hurricane winds. Although the hurricane wind field is directed not only cyclonically about the storm but also radially inward, the net radial movement of surface layer water is outward due to the Coriolis effect. A vertical-radial circulation, consisting of intense upwelling within the radius of maximum hurricane winds and weaker downwelling at greater radial distance is produced by mass continuity. As a result of this circulation, the ocean temperatures near the center of the storm decrease throughout the stable part of the water column that lies below the mixed layer. The ocean surface temperatures are also affected if the upwelling water reaches the surface.

There is also an important mixing effect due to the hurricane force winds, as indicated by the model studies of Elsberry, Fraim and Trapnell (1976) and Chang and Anthes (1978). Mechanical and convective

generation of turbulent kinetic energy in the upper ocean tend to achieve maximum values at the radius of maximum winds. As a result, the relatively warm surface water is cooled and the coler water immediately below the initial mixed layer depth is warmed as it is entrained into and is mixed with the surface water. The combination of the advective effects and mixing effects described above is clearly quite complex and requires high vertical and horizontal resolution to simulate.

To simplify the testing of the present model, the forcing due to a stationary, axisymmetric hurricane is used. A 4.5 km horizontal grid spacing is utilized in order to have 10 grid points within the radius of maximum winds which is located at 45 km (Fig. 1). The ocean is initially at rest with a uniform surface temperature of 30^{o}C and a uniform mixed layer depth of 60 m. To reduce the initial shock, the hurricane forcing is slowly spun up to full intensity over the first 12 h.

The evolution predicted at 12 h and 24 h with the embedded mixed layer-ocean circulation model is presented in Figs. 3a-d and Figs. 4a-d, respectively. Because of the explicit mixed layer, the surface inputs of heat and momentum are distributed over a deep layer. Thus, the maximum v component at 12 h (Fig. 3a) is rather small considering the large magnitude of the surface stress near the center (Fig. 1). At 12 h there is a deep layer of cyclonically rotating water in the mixed layer and a very small and weak anticyclonic circulation below the mixed layer. A region of relatively weak outward flow is predicted (Fig. 3b) for the mixed layer in the inner region. The compensating inward flow below is a maximum near the top of the thermocline. As is

indicated by the packing of the w-isolines at the center of the hurricane in Fig. 3c, the associated vertical motion at 12 h is concentrated in a very narrow zone. The temperature field at 12 h in Fig. 3d is beginning to show the effect of the strong upwelling near the center. Toward the center, the isotherms are tilted upward at progressively larger angles. The 29°C isotherm has been lifted about 15 m near the storm center.

At 24 h the tangential (v) components within the mixed layer near the center are only slightly stronger than at 12 h. A maximum value of less than 1 m s^{-1} is qualitatively in agreement with the largest currents measured as hurricane Eloise passed an instrumented oil rig off the coast of Louisiana (Forristall, 1980). Although the strength of the hurricane forcing used here is somewhat larger than in Eloise, there is a compensating effect due to the larger layer depth in the model compared to the pre-Eloise ocean conditions of between 30 and 45 m. At larger r, there is a region of weak, anticyclonic flow that is produced as the water moves outward while tending to conserve angular momentum. The radial extent of the outward flow near the surface in Fig. 4b is much greater than at 12 h. The maximum of this radial component is nearly as large as the corresponding tangential component, so that the current direction is approximately 40° relative to a circle, or 60° to the right of the surface stress. The compensating inflow occurs over a deep layer, although the maximum is clearly located in the upper layers of the thermocline beneath the radius with maximum stress. The primary upwelling at 24 h remains at the center of the hurricane and extends to great depths (only the upper layers of the model are shown here). A much weaker descent occurs at large r to compensate for

the surface flow, which has reached the outer boundary by 24 h. The primary feature in the temperature field at 24 h (Fig. 4d) is the expansion of the zone of upwelled water, which has surfaced near the center and has been advected outward.

The advective effect near the center of the hurricane is so dominant that it is difficult to isolate the mixing effect. Deviations of the predicted temperature fields at 12 h and 24 h from the initial values are shown in Figs. 5a and 5b, respectively. After 12 h, the maximum temperature decrease occurs near the storm center in association with the strong upwelling there, while a region of temperature increase occurs near the outer boundary due to downwelling. There is a second zone of increased temperatures at the base of the mixed layer, which has deepened as a result of both entrainment and vertical advection. A similarly shaped region of temperature increase is found somewhat farther from the center of the 24 h field shown in Fig. 5b. Such a region of temperature decrease above the initial mixed layer base and increase below it is an indication of entrainment mixing. It is clear from the above temperature changes that in the present case of stationary forcing, advective effects dominate the heat budget. If the hurricane was translating, upwelling at a point would be followed by downwelling and the advective effects would have a tendency to cancel. In such a case, the mixing effects would be relatively more important in producing a permanent change in the thermal structure.

The explicit treatment of the dynamics of the mixed layer in the embedded model results in a temperature field that is similar to observations of oceanic response to hurricanes (e.g. Leipper, 1967). The purpose of the limited test shown here is only to demonstrate that the

embedding procedure proposed here appears to be capable of treating both the mixing effects and the advective effects in a numerically efficient and physically realistic manner. No inference should be made regarding the viability of different mixing parameterizations.

8. CONCLUDING REMARKS

This paper has addressed the problem of developing a dynamical ocean circulation model capable of treating both advective and mixing effects in response to realistic atmospheric forcing. The solution presented here is the embedding of a bulk mixed layer model within a multi-level primitive equation model. In addition, the traditional "convective adjustment" often used in such primitive equation models has been replaced by a more general dynamical stability condition. The resulting model is an attempt to combine the advantages of layer models and level models into a single model.

Other approaches to the problem are clearly possible. One alternative approach is to use a higher order diffusion model in which the vertical eddy viscosity and conductivity are expressed as functions of the model variables. This approach has been utilized by Madala and Piacsek (1977) using the popular formulas of Munk and Anderson (1948). With such an approach, high vertical resolution is necessary in order to represent the sharp transition between the highly turbulent surface layer and the weakly turbulent, highly stratified region below. Another alternative approach is to develop a multi-layer model which includes turbulent exchange between the layers. A bulk mixed layer could be considered as the uppermost layer in such a model. One of the results of the present study suggests that, with this approach, there

should also be a turbulent transfer of momentum between the layers, an effect that has not been generally included in layer models before.

The example of the oceanic response to a stationary, axisymmetric hurricane examined here is an extreme test of the present embedded model because both the advective and the mixing effects are very strong. Additional studies with the present model are currently in progress. These include the ocean's response to a variety of strong atmospheric forcing situations and the response of an upper ocean density front to local atmospheric forcing. A three dimensional version of the model is being used to study a variety of oceanic mesoscale features as well as large-scale interannual variability (anomalies) in the central North Pacific Ocean. These studies suggest that the embedded model is capable of simulating the ocean's response to a wide range of oceanic and atmospheric forcing conditions. Other tests, including comparisons with observational data, are planned to further validate the present model. As a result, it now appears that the model can serve as a useful tool to increase our understanding of, and eventually our ability to predict, a variety of oceanic phenomena that involve both advective and mixing processes.

Acknowledgements. The authors would like to thank the Naval Postgraduate School Foundation Research Program for the initial funding, and the Office of Naval Research, Ocean Science Branch, for continued funding under contract number NR083-275, N00014-79-WR-90020. Computer time was provided by the Church Computer Center at the Naval Postgraduate School, including the graphics package which was supplied by the National Center for Atmospheric Research.

The authors would also like to thank Joanne Kallweit and Jeanine Washington for their expert help in expediting computer turnaround, and Ms Marion Marks for her careful typing of the manuscript.

APPENDIX

Space finite differencing

The numerical scheme makes use of centered space differencing on a staggered grid. In the notation which follows, the letters j and k are integers. The vertical index is k and the variables u, v, T and $\hat{p}$ are defined at level k, k=1, ...K, while the vertical velocity w is defined at the K-1 interfaces between the levels and also at the top and bottom of the ocean where it is zero. Standard difference notation is utilized in which for example $\delta_x(q)_{i+1/2,j} = q_{i+1,j} - q_{i,j}$ and $(\bar{q}^x)_{i+1/2,j} = 1/2\ (q_{i+1,j} + q_{i,j})$.

Let ΔZ_k, k=1,...K, be the specified thickness of the k th level and

$$Z_{k+1/2} = -\sum_{\ell=1}^{k} \Delta Z_\ell \quad ; \quad k=1, \ldots K \tag{A1}$$

be the value of Z at the base of the k th level ($Z_{1/2} = 0$ and $Z_{K+1/2} = -H$). Average layer thicknesses are defined by

$$\Delta Z_{k+1/2} = (\bar{\Delta Z}^{z})_{k+1/2} \quad ; \quad k=1, \ldots K-1 \ , \tag{A2}$$

and average layer heights are defined by

$$Z_k = (\bar{Z}^{z})_k \quad ; \qquad k=1, \ldots K \ . \tag{A3}$$

The finite-difference analog of (2.13) is

$$\hat{p}_k = p_k - \tilde{p} \ , \tag{A4}$$

where the wavy overbar denotes the finite-difference vertical average

$$\tilde{(\ )} = \frac{1}{H} \sum_{k=1}^{K} (\ )_k \Delta Z_k \ , \tag{A5}$$

and

$$\left.\begin{aligned} p_1 &= 0 \\ p_k &= \sum_{\ell=1}^{k-1} \rho_o [1-\alpha((\tilde{T}^z)_{\ell+\frac{1}{2}} - T_o)] g \Delta Z_{\ell+\frac{1}{2}} \ ; \quad k=2, \ \ldots \ K \end{aligned}\right\} . \tag{A6}$$

Thus, $\hat{p}_k$ is the thermally induced hydrostatic pressure field which has a zero vertical average.

Let Δr be the (constant) horizontal grid size. Then the velocity components u and v are defined at the center of the grid intervals located at the points

$$r_j = \frac{1}{2} \Delta r + (j-1) \Delta r \ ; \quad j=1, \ \ldots \ J \ . \tag{A7}$$

The variables T, $\hat{p}$ and w are defined at the J-1 interfaces and at both ends of the domain (r=0 and R). These points are located at

$$\left.\begin{aligned} r_{\frac{1}{2}} &= 0 \\ r_{j+\frac{1}{2}} &= (\tilde{r}^r)_{j+\frac{1}{2}} \ ; \qquad j=1, \ \ldots \ J-1 \\ r_{J+\frac{1}{2}} &= R \end{aligned}\right\} . \tag{A8}$$

In addition, the space differencing scheme makes use of the following definitions of the grid volumes.

$$\left.\begin{aligned} \pi_{\frac{1}{2},k} &= \frac{1}{2}\, r_1\, \Delta r\, \Delta Z_k \\ \pi_{j+\frac{1}{2},k} &= r_{j+\frac{1}{2}}\, \Delta r\, \Delta Z_k \quad ; \quad j=1, \ldots J \\ \pi_{j,k} &= (\bar{\pi}^{r})_{j,k} \quad ; \qquad j=1, \ldots J \end{aligned}\right\} \quad . \tag{A9}$$

The finite-difference analog of the continuity equation (2.4) is

$$\delta_r(u^*)_{j+\frac{1}{2},k} + \delta_z(w^*)_{j+\frac{1}{2},k} = 0 \quad ; \quad j=0, \ldots J \ , \tag{A10}$$

where

$$\left.\begin{aligned} u^*_{j,k} &= u_{j,k}\, r_j\, \Delta Z_k \\ w^*_{j+\frac{1}{2},k+\frac{1}{2}} &= w_{j+\frac{1}{2},k+\frac{1}{2}}\, r_{j+\frac{1}{2}}\, \Delta r \end{aligned}\right\} \quad . \tag{A11}$$

The finite difference analog of the boundary conditions which are needed to apply (A10), and the equations to follow, on the boundaries are given in the next section.

The finite-difference analog of the thermal energy equation (2.3) and the prognostic equation for the mixed layer depth (2.15) are

$$\frac{\partial}{\partial t}\left(T_{j+\frac{1}{2},k}\ \pi_{j+\frac{1}{2},k}\right) = -\ \delta_r(Tu)^*_{j+\frac{1}{2},k} - \delta_z(Tw)^*_{j+\frac{1}{2},k} + \delta_r(Tr)_{j+\frac{1}{2},k} - \delta_z(\overline{w'T'})^*_{j+\frac{1}{2},k} \tag{A12}$$

$$\frac{\partial}{\partial t}\left(h_{j+\frac{1}{2}}\ r_{j+\frac{1}{2}}\ \Delta r\right) = -\ \delta_r(hu)^*_{j+\frac{1}{2}} + (w_e)_{j+\frac{1}{2}}\ r_{j+\frac{1}{2}}\ \Delta r\ , \tag{A13}$$

where

$$\left.\begin{aligned}
(Tu)^*_{j,k} &= (\bar{T}^r)_{j,k}\ u^*_{j,k} \\
(Tw)^*_{j+\frac{1}{2},k+\frac{1}{2}} &= (\bar{T}^z)_{j+\frac{1}{2},k+\frac{1}{2}}\ w^*_{j+\frac{1}{2},k+\frac{1}{2}} \\
(Tr)_{j,k} &= A_T\ \delta_r(T)_{j,k}\ r_j\ \Delta Z_k/\Delta r \\
(\overline{w'T'})^*_{j+\frac{1}{2},k+\frac{1}{2}} &= (\overline{w'T'})_{j+\frac{1}{2},k+\frac{1}{2}}\ r_{j+\frac{1}{2}}\ \Delta r \\
(hu)^*_j &= (\bar{h}^r)_j\ u^*_{j,1}
\end{aligned}\right\} \tag{A14}$$

The finite-difference analog of the radial component of the equation of motion (2.11) is

$$\begin{aligned}
\frac{\partial}{\partial t}\left(u_{j,k}\ \pi_{j,k}\right) = &-\ \delta_r(uu)^*_{j,k} - \delta_z(uw)^*_{j,k} \\
&+ (f + v_{j,k}/r_j)v_{j,k}\ \pi_{j,k} - \delta_r(\hat{p})_{j,k}\ r_j\ \Delta Z_k/\rho_o \\
&+ \delta_r(ur)_{j,k} - \delta_z(\overline{w'u'})^*_{j,k} - (uB)_{j,k}
\end{aligned} \tag{A15}$$

where,

$$
\left.
\begin{aligned}
(uu)^{*}_{j+\frac{1}{2},k} &= (\bar{u}^{r})_{j+\frac{1}{2},k}\,(u^{-*1})_{j+\frac{1}{2},k} \\
(uw)^{*}_{j,k+\frac{1}{2}} &= (\bar{u}^{z})_{j,k+\frac{1}{2}}\,(\bar{w}^{*r})_{j,k+\frac{1}{2}} \\
(ur)_{j+\frac{1}{2},k} &= A_M\,\delta_r(u)_{j+\frac{1}{2},k}\; r_{j+\frac{1}{2}}\,\Delta Z_k/\Delta r \\
(\overline{w'u'})^{*}_{j,k+\frac{1}{2}} &= (\overline{w'u'})_{j,k+\frac{1}{2}}\; r_j\,\Delta r \\
(uB)_{j,k} &= \frac{\Delta Z_k}{H}\sum_{k=1}^{K}\{-[\delta_r(uu)^{*}_{j,k}] \\
&\quad + \frac{v^2_{j,k}\,\pi_{j,k}}{r_j} + \frac{(\tau_r)_j\,\pi_{j,k}}{\rho_o H}
\end{aligned}
\right\} . \qquad \text{(A16)}
$$

The finite-difference analog of the tangential component of the equation of motion (2.12) has a similar form.

Boundary conditions

The lateral boundary conditions will only be given for r=0 since the conditions at r=R are similar. The variables and T,$\hat{p}$ and w are defined at grid points which coincide with the lateral boundaries while (u,v) are defined at points located one-half grid distance inside the boundary. Thus, the variables $r_{1/2}$, $T_{1/2,k}$, $\hat{p}_{1/2,k}$ and $w_{1/2,k+1/2}$ are located at the origin while r_1, $u_{1,k}$ and $v_{1,k}$ are located one-half grid distance from the origin.

The zero normal flux condition at r = 0 is maintained by imposing the following antisymmetric condition on the normal flux:

$$u^{*}_{0,k} = - u^{*}_{1,k} , \qquad \text{(A17)}$$

while the condition of no lateral eddy flux of heat and momentum at r = 0, which is used in (A12) and (A15), is given by

$$\left.\begin{aligned} (Tr)_{0,k} &= -(Tr)_{1,k} \\ (ur)_{\frac{1}{2},k} &= (vr)_{\frac{1}{2},k} = 0 \end{aligned}\right\} . \tag{A18}$$

Equations (A17) and (A18) are the finite-difference analogs of (2.7).

The finite-difference analogs of the boundary conditions on w in (2.8) are

$$w^*_{j+\frac{1}{2},\frac{1}{2}} = w^*_{j+\frac{1}{2},K+\frac{1}{2}} = 0 . \tag{A19}$$

The finite-difference analog of the boundary conditions on the surface fluxes in (2.9) and (2.10) are

$$\left.\begin{aligned} -(\overline{w'T'})^*_{j+\frac{1}{2},\frac{1}{2}} &= (Q_{j+\frac{1}{2}}/\rho_o C)\ r_{j+\frac{1}{2}}\ \Delta r \\ -(\overline{w'u'})^*_{j,\frac{1}{2}} &= ((\tau_r)_j/\rho_o)\ r_j\ \Delta r \\ -(\overline{w'v'})^*_{j,\frac{1}{2}} &= ((\tau_\theta)_j/\rho_o)\ r_j\ \Delta r \end{aligned}\right\} , \tag{A20}$$

and

$$(\overline{w'T'})^*_{j+\frac{1}{2},K+\frac{1}{2}} = (\overline{w'u'})^*_{j,K+\frac{1}{2}} = (\overline{w'v'})^*_{j,K+\frac{1}{2}} = 0 , \tag{A21}$$

respectively, where the forcing functions Q, τ_r and τ_θ are taken from Fig. 1.

Vertical diffusion

In this section, and the ones to follow, the numerical methods used to calculate the turbulent fluxes in (A12), (A13) and (A15) are given. The vertical flux of heat and momentum due to eddy diffusion is calculated at the top and bottom (interface) of the model level which contains the mixed layer depth and at the top and bottom of every model level which lies entirely below the mixed layer. That part of the turbulent fluxes in (A12) and (A15) which is due to vertical diffusion is calculated from

$$(\overline{w'T'})^{*}_{j+\frac{1}{2},k+\frac{1}{2}} = - K_T \, \delta_z(T)_{j+\frac{1}{2},k+\frac{1}{2}} \, r_{j+\frac{1}{2}} \, \Delta r/\Delta Z_{k+\frac{1}{2}}$$

$$(\overline{w'u'})^{*}_{j,k+\frac{1}{2}} = - K_M \, \delta_z(u)_{j,k+\frac{1}{2}} \, r_j \, \Delta r/\Delta Z_{k+\frac{1}{2}} \qquad \text{(A22)}$$

with a similar equation for $(\overline{w'v'})$.

Boundary layer entrainment

This section concerns the numerical treatment of entrainment by the embedded mixed-layer model. In a time step Δt, the amount of mixed layer deepening and the associated layer temperature change depend upon both the prior thermal structure and the entrainment heat flux $(\overline{w'T'})_{-h}$, computed by solving (4.1) simultaneously with (4.2) and (4.3). Following (6.2), heat is vertically redistributed, and the changes in mixed layer temperature and depth are found as illustrated by Fig. A1 in which

i) $\delta T = (\overline{w'T'})_{-h} \, \Delta t/h$

ii) δh is determined by requiring

$$\text{area } B = \text{area } A = h\,\delta T \ .$$

Only after applying this entrainment mixing is the new mixed layer temperature further adjusted to account for the net surface heat flux, $(\overline{w'T'})_o$ (although $(\overline{w'T'})_o$ helped to determine the value of δT above through its appearance in the turbulent kinetic energy equation, (4.3)). Once the new mixed layer depth is determined, the horizontal components of mixed layer velocity are adjusted so as to conserve momentum and preserve vertical homogeneity in the mixed layer.

Boundary layer shallowing

When the depth of the turbulent boundary layer decreases, it leaves behind a remnant mixed layer structure. In a numerical simulation of this event, unless the base of the older mixed layer exactly coincides with an interface between two model levels, some information must be lost because only one mixed layer depth is retained. This loss of information is a potentially serious problem because such remnant mixed layer structures influence the potential energy in the column. In the present model, when the mixed layer depth is predicted to decrease, from h to h' say, the temperature in the model levels which lie partly or entirely within the mixed layer are adjusted along with the temperature in the model level immediately below the mixed layer depth (Fig. A2). This adjustment is given by

$$[T_{\ell}']_{\ell=1,k} = T_{k+1} + \frac{h(T_k - T_{k+1})[D_k - h + D_m]}{D_k D_m} \tag{A23}$$

$$T_{k+1}' = T_{k+1} + \frac{h(T_k - T_{k+1})[h - D_m]}{D_k \Delta z_k} \tag{A24}$$

$$\left.\begin{aligned} D_k &= \sum_{\ell=1}^{k} \Delta z_{\ell} \\ D_m &= \mathrm{Max}(h', D_{k-1}) \end{aligned}\right\} , \tag{A25}$$

where k is the model level which contained the original mixed layer depth before shallowing, T_k and h are the model temperatures and mixed layer depth before shallowing, while T_k' is the adjusted model temperatures after shallowing. It can be shown that the above adjustment of temperatures conserves both heat and potential energy.

The procedure is illustrated in Fig. A2. A slight vertical redistribution of heat enables the conservation of potential energy. In the case when the new turbulent boundary layer, h', is shallower than

$$D_{k-1} = \sum_{\ell=1}^{k-1} \Delta z_{\ell} ,$$

the new mixed layer depth will not be apparent in the temperature profile until the turbulent boundary layer is sufficiently warmed

by a net flux of heat and radiation at the surface. In the illustration, area C + area D = area E. In this purposely exaggerated example, the surface temperature is seen to rise a slight amount. However, over a cycle of deepening shallowing and deepening again, there will be no net change in surface temperature.

Dynamic stability condition

This stability condition, which is a simple generalization of the familiar "convective adjustment", is imposed by examining the value of the Richardson number, Ri, defined at the interface between model levels given below. If the inequality in (A26) is not satisfied, the temperature and the velocity components in the two adjacent levels are "dynamically adjusted" in accordance with the following four assumptions:

(i) heat is conserved,

(ii) momentum is conserved,

(iii) dynamic stability is imposed between the two levels by requiring that the Richardson number

$$Ri = \frac{\alpha g \, \Delta z_{k+\frac{1}{2}} \, \Delta T}{(\Delta u)^2 + (\Delta v)^2} \geq (Ri)_{CR} = .25 \, , \tag{A26}$$

(iv) the mixing ratios for heat and momentum are equal, i.e.

$$\frac{T_k - T'_k}{T_k - \bar{T}} = \frac{T_{k+1} - T'_{k+1}}{T_{k+1} - \bar{T}} = \frac{u_k - u'_k}{u_k - \bar{u}} =$$

$$= \frac{u_{k+1} - u'_{k+1}}{u_{k+1} - \bar{u}} = \frac{v_k - v'_k}{v_k - \bar{v}} = \frac{v_{k+1} - v'_{k+1}}{v_{k+1} - \bar{v}} \, , \tag{A27}$$

where the prime denotes the new, adjusted value. In these expressions, ΔT, Δu and Δv are the vertical differences of heat and momentum, $T_k - T_{k+1}$ etc., while $\bar{T}$, $\bar{u}$ and $\bar{v}$ represent the weighted vertical average of the two levels, $0.5(T_k \Delta Z_k + T_{k+1} \Delta Z_{k+1})/\Delta Z_{k+1/2}$ etc. The above stability condition is calculated at the velocity points in the model, and therefore, because of the staggered grid, the temperatures appearing in (A26) and (A27) are two grid-point averages. Consequently, a weighted average of the temperature adjustment determined from the above conditions is used to compute the adjustments that are applied at the temperature grid points. With some straightforward algebraic manipulations it can be shown that the unique solution to conditions (i) through (iv) is

$$\left.\begin{aligned} T'_k &= \bar{T} + \gamma\Delta T \\ T'_{k+1} &= \bar{T} - \xi\gamma\Delta T \\ u'_k &= \bar{u} + \gamma\Delta u \\ u'_{k+1} &= \bar{u} - \xi\gamma\Delta u \\ v'_k &= \bar{v} + \gamma\Delta v \\ v'_{k+1} &= \bar{v} - \xi\gamma\Delta v \end{aligned}\right\} , \qquad \text{(A28)}$$

where

$$\gamma = \frac{Ri}{(Ri)_{CR}(1+\xi)} \quad \text{and} \quad \xi = \frac{\Delta Z_k}{\Delta Z_{k+1}} .$$

If the mixing ratios in (A27) are denoted by m , it can easily be shown that

$$m = 1 - \frac{Ri}{(Ri)_{CR}} ; \qquad 0 < Ri \leq (Ri)_{CR}$$

$$m = 1 ; \qquad Ri \leq 0 . \tag{A29}$$

Complete mixing between two levels, as defined by m=1, occurs only if the value of the Richardson number before mixing is less than or equal to zero.

Time integration

Time integration is performed using the leapfrog scheme with an Euler-backward scheme introduced at the start and at every 11 timesteps thereafter to remove any solution separation in time. The forward differencing scheme, however, is used for the eddy diffusion and turbulent mixing terms. As indicated in Section 6, the calculation of the advection and diffusion terms is split from the calculation of the turbulent mixing terms.

Suppose the dependent variables u,v,T and h are known at the two consecutive time levels n-1 and n. When using the leapfrog scheme, the first step is to calculate the pressure $\hat{p}$ and the vertical velocity w^* using (A4) and (A10) and the values of T, u and v at time level n. Next, the dynamical terms on the right hand side of (A12), (A13) and (A15) are calculated, also using the variables at time level n. These dynamical terms include the horizontal advection of u,v,T and h; the vertical advection of u,v and T; the Coriolis acceleration; the centripetal acceleration; and the pressure gradient force. Next, the horizontal and vertical

diffusion terms are calculated using u,v and T at time level n-1 and are added to the dynamical terms. The coupling procedure given by (6.1) is then applied to these accumulated tendencies which are then multiplied by $2\Delta t$ and added to the value of the variable at time level n-1. This partially advances the fields to the new time level n+1. The dynamic stability condition (see above and in Section 5) is then imposed and the variables within the mixed layer are vertically averaged above the new mixed layer depth. Finally, the tendencies due to the surface fluxes (A20) and turbulent mixing (Section 4) are calculated and the fields are advanced to their final value at the time level n+1.

When the two step Euler-backward integration scheme is used, the sequence of calculations is the same as described above in both the "forward" and the "backward" steps. The only difference is that the diffusion terms are no longer lagged in time but are calculated from the same fields as the dynamical terms.

REFERENCES

Bryan, K., 1979. Models of the world ocean. Dyn. Atmos. Oceans, 3:327-338.

Chang, S. W. and R. A. Anthes, 1978. Numerical simulations of the ocean's nonlinear baroclinic response to translating hurricanes. J. Phys. Oceanogr., 8:468-480.

DeSzoeke, R. A. and P. B. Rhines, 1976. Asymptotic regimes in mixed layer deepening. J. Mar. Res., 34:111-116.

Elsberry, R., T. Fraim and R. Trapnell, Jr., 1976. A mixed layer model of the oceanic thermal response to hurricanes. J. Geophys. Res., 81:1153-1162.

Forristall, G. Z., 1980. A two-layer model of hurricane-driven currents on an irregular grid. J. Phys. Oceanogr., 10:1417-1438.

Garwood, R. W., Jr., 1976. A general model of the ocean mixed layer using a two-component turbulent kinetic energy budget with mean turbulent field closure. NOAA-TR-ERL-384, 95 pp., NTIS, Department of Commerce, Springfield, VA.

Garwood, R. W., Jr., 1977. An oceanic mixed layer model capable of simulating cyclic states. J. Phys. Oceanogr., 7:455-468.

Garwood, R. W., Jr., 1979. Air-sea interaction and dynamics of the surface mixed layer. Rev. Geophys. Space Phys., 17:1507-1524.

Garwood, R. W., Jr. and D. A. Adamec, 1980. Model simulation of seventeen years of mixed layer evolution at Ocean Station Papa, 1953-1969. Tech. Rept. Naval Postgraduate School (in preparation).

Garwood, R. W., Jr. and J-Y Yun, 1979. Bulk closure for the oceanic planetary boundary layer: a realistic and numerically efficient model. Proc. 2nd Symp. Turbulent Shear Flows, Imperial College, London, July 2-4.

Haney, R. L., 1979. Numerical models of ocean circulation and climate interaction. Rev. Geophys. Space Phys., 17:1494-1507.

Holland, W. R., 1979. The general circulation of the ocean and its modelling. Dyn. Atmos. Oceans, 3:111-142.

Kraus, E. B., editor, 1977. Modelling and Prediction of the Upper Layers of the Ocean. Proc. of NATO Advanced Study Institute, Urbino, Italy, 1975, Pergamon Press, 375 pp.

Leipper, D. F., 1967. Observed ocean conditions and hurricane Hilda, 1964. J. Atmos. Sci., 24:182-196.

Madala, R. V. and S. A. Piacsek, 1977. A semi-implicit numerical model for baroclinic oceans. J. Comp. Phys., 23:167-178.

Munk, W. and E. R. Anderson, 1948. Notes on a theory of the thermocline. J. Marine Res., 7:276-295.

National Academy of Sciences, 1975. Numerical Models of Ocean Circulation. NAS, Washington, DC, 20418, 364 pp.

Niiler, P. P., 1975. Deepening of the wind-mixed layer. J. Marine Res., 33:405-422.

O'Brien, J. J. and R. O. Reid, 1967. The non-linear response of a two-layer, baroclinic ocean to a stationary, axially-symmetric hurricane: Part I. Upwelling induced by momentum transfer. J. Atmos. Sci., 24:197-207.

Pollard, R. T., P. Rhines and R. Thompson, 1973. The deepening of the wind-mixed layer. Geophys. Fluid Dyn., 3:381-404.

Robinson, A. R., D. E. Harrison and D. B. Haidvogel, 1979. Mesoscale eddies and general ocean circulation models. Dyn. Atmos. Oceans, 3:143-180.

Thompson, R.O.R.Y., 1976. Climatological numerical models of the surface mixed layers of the ocean. J. Phys. Oceanogr., 6:496-503.

WMO/ICSU, Report of the JOC/SCOR Joint Study Conference on General Circulation Models of the Ocean and their Relation to Climate. Helsinki, 23-27 May 1977, Vols. I and II, WMO, Geneva.

TABLE 1

Symbol	Value	Description
A_M	2×10^8 cm^2 s^{-1}	Horizontal eddy viscosity
A_T	4×10^7 cm^2 s^{-1}	Horizontal eddy conductivity
K_M	.5 cm^2 s^{-1}	Vertical eddy viscosity
K_T	.5 cm^2 s^{-1}	Vertical eddy conductivity
α	2×10^{-4} deg^{-1}	Thermal expansion coefficient
T_o	5°C	Reference temperature
ρ_o	1.0276 gm cm^{-3}	Reference density
f	6×10^{-5} s^{-1}	Coriolis parameter
Δr	4.5 km	Horizontal grid size
r_m	45 km	Radius of maximum winds
R	450 km	Domain extent
H	964 m	Depth of ocean
Δt	150 s	Time step

FIGURE CAPTIONS

Fig. 1. Forcing functions for the ocean model, each normalized by the value of the function at the radius of maximum winds. The tangential and radial stress components have the same form (solid line) with maximum values of 35.9 and -12.9 dPa, respectively. The surface heat flux (dashed) has a maximum value of $-840\ Wm^{-2}$.

Fig. 2. Schematic illustration of the embedded mixed layer of depth h, located within the k th level in the circulation model. See Section 6 for a complete discussion of the embedding technique.

Fig. 3. Predicted oceanic response after 12 h to the hurricane forcing in Fig. 1 using the circulation model with the embedded mixed layer. Only the upper 150 m is shown, with the center of the hurricane (r=0) on the left and each larger tick mark on the abscissa corresponding to 45 km. (a) Tangential current component (cyclonic flow, dashed) with contour interval of $0.1\ m\ s^{-1}$. (b) Radial current component (inflow, dashed) with contour interval $0.1\ m\ s^{-1}$. (c) Vertical velocity (downward flow, dashed) with contour interval of $1\ m\ h^{-1}$. (d) Temperature contours (^{o}C).

Fig. 4. Similar to Fig. 3 except at 24 h.

Fig. 5. Temperature deviations (contour interval 0.5°C, negative values dashed) from the initial state predicted by the embedded mixed layer model after (a) 12 h and (b) 24 h.

Fig. A1. An example of mixed layer deepening and cooling by entrainment. The original structure prior to entrainment (solid line) had a mixed layer depth of 36 m, mixed layer temperature of 22.5°C and temperature jump at the base of the layer of approximately 2.6°C. The mixed layer deepened by entrainment to below 40 m, the mixed layer temperature decreased to 22.2°C and the temperature jump at the base of the layer decreased to approximately 2.4°C (dashed line). Heat is conserved, so area A = area B.

Fig. A2. An example of mixed layer shallowing. The original temperature structure prior to shallowing (solid line) is the same as in Fig. A1. In this example, the mixed layer shallowed to a new depth which lies above the k th level, but which will not be apparent in the temperature structure (dashed line) until there is a downward flux of heat at the surface. The new temperature structure was obtained from (A23)-(A25) and is such that area C + area D = area E.

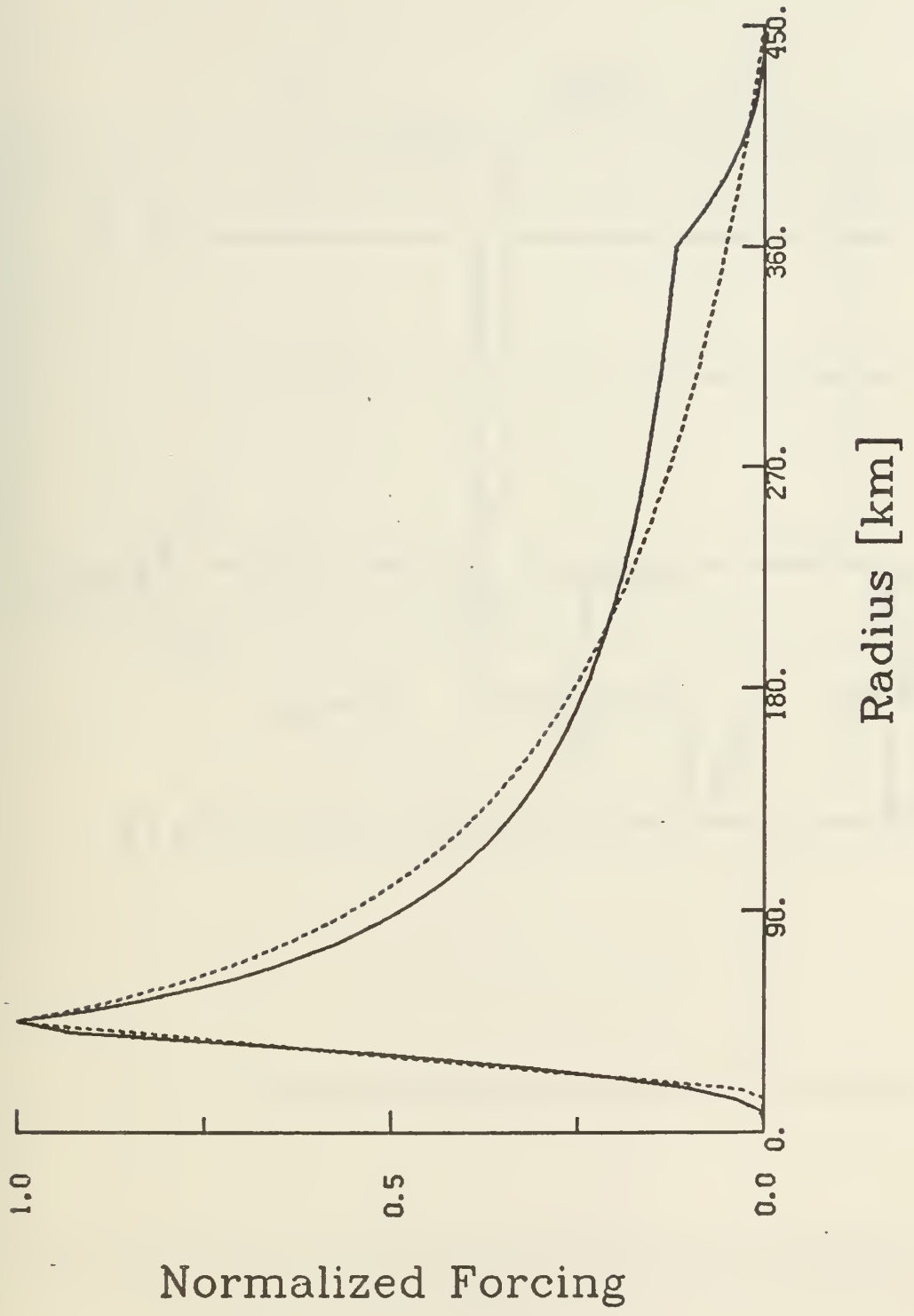
1.0
0.5
0.0
0.
90.
180.
270.
360.
450.
Radius [km]
Normalized Forcing

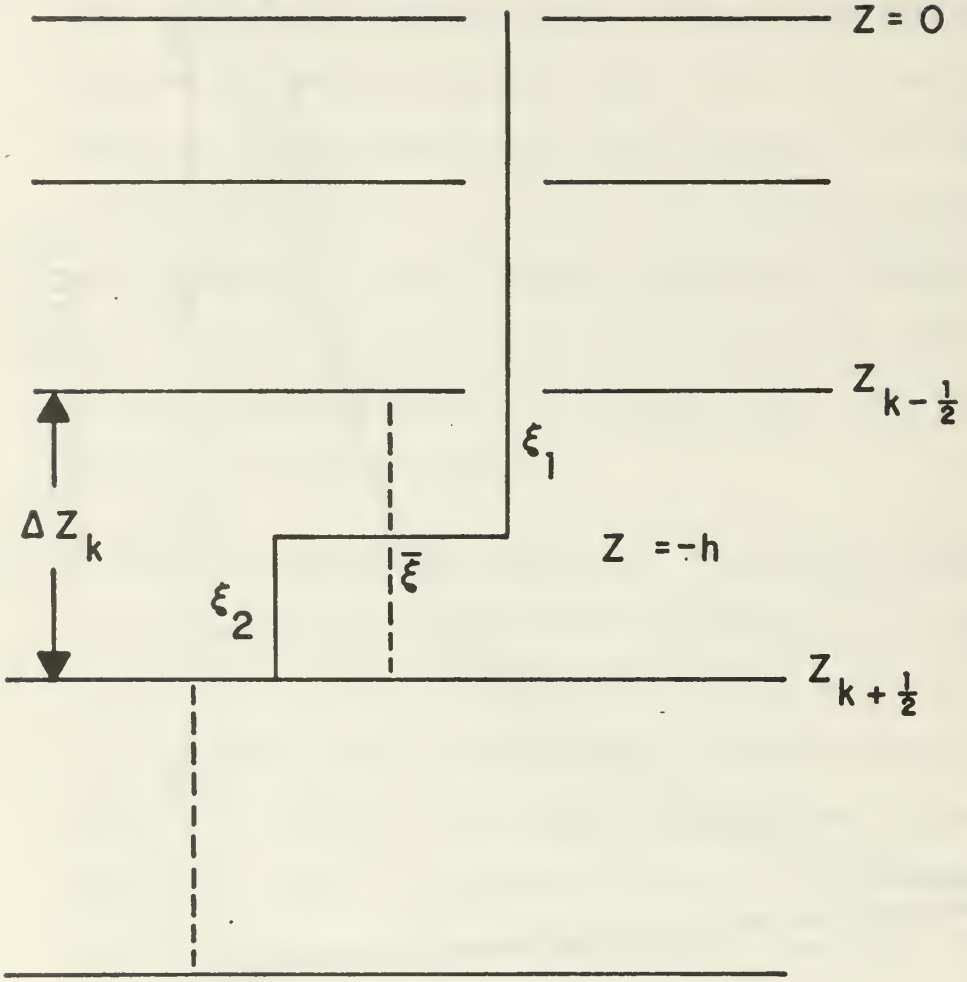
Z = 0
$Z_{k-\frac{1}{2}}$
ξ_1
ΔZ_k
Z = -h
$\bar{\xi}$
ξ_2
$Z_{k+\frac{1}{2}}$

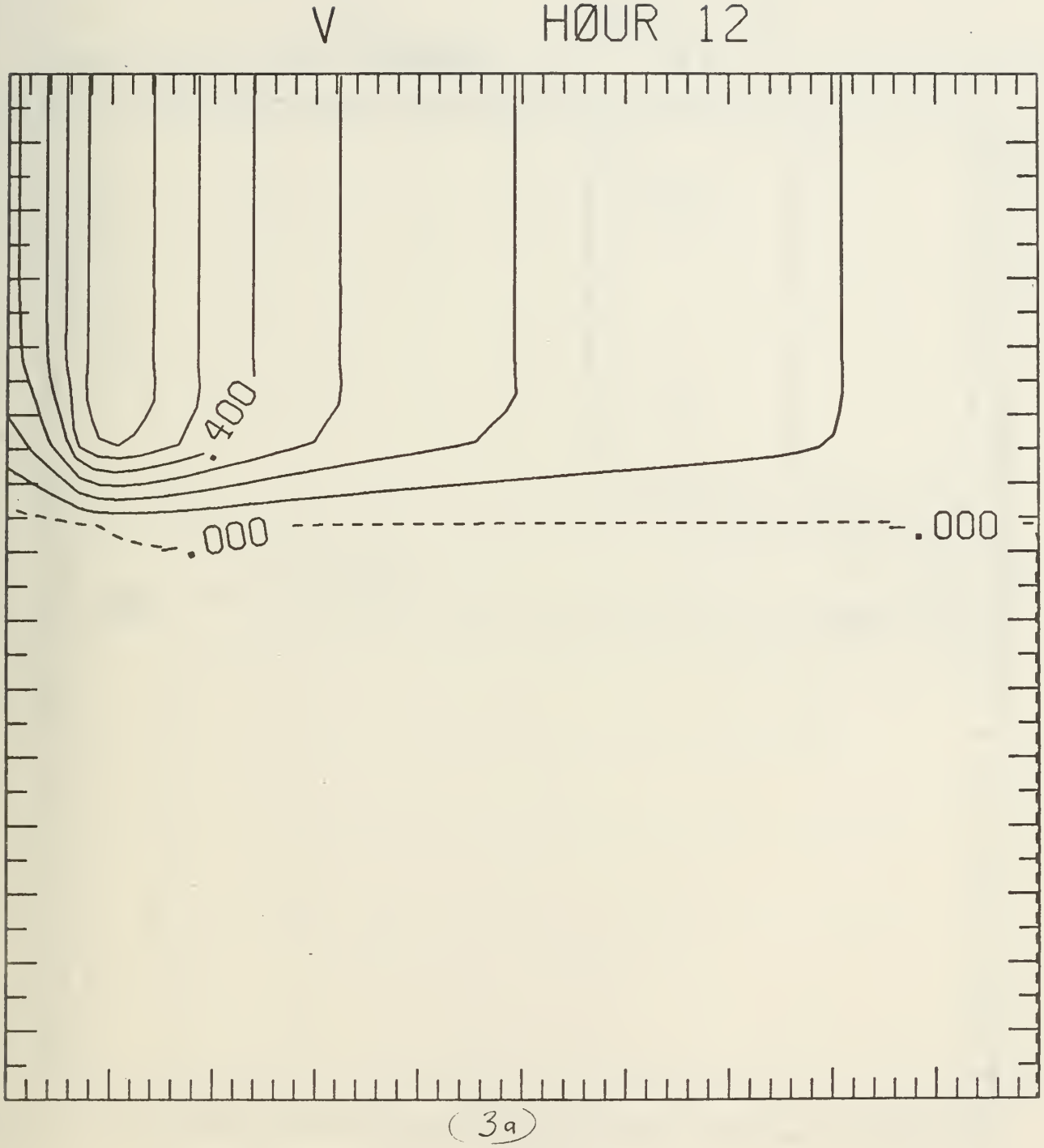

(3a)

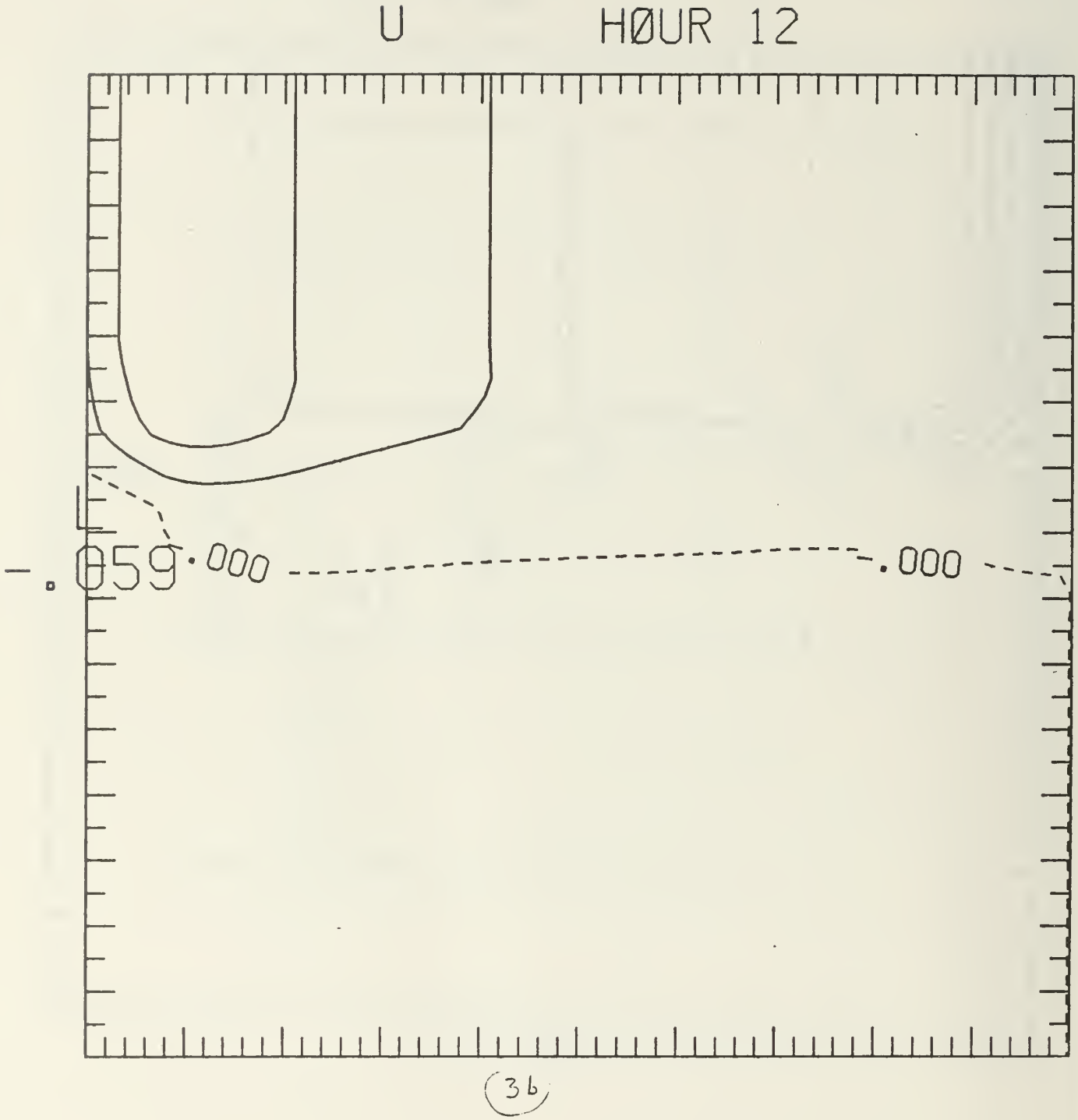
U
HØUR 12
.059
.000
.000
36

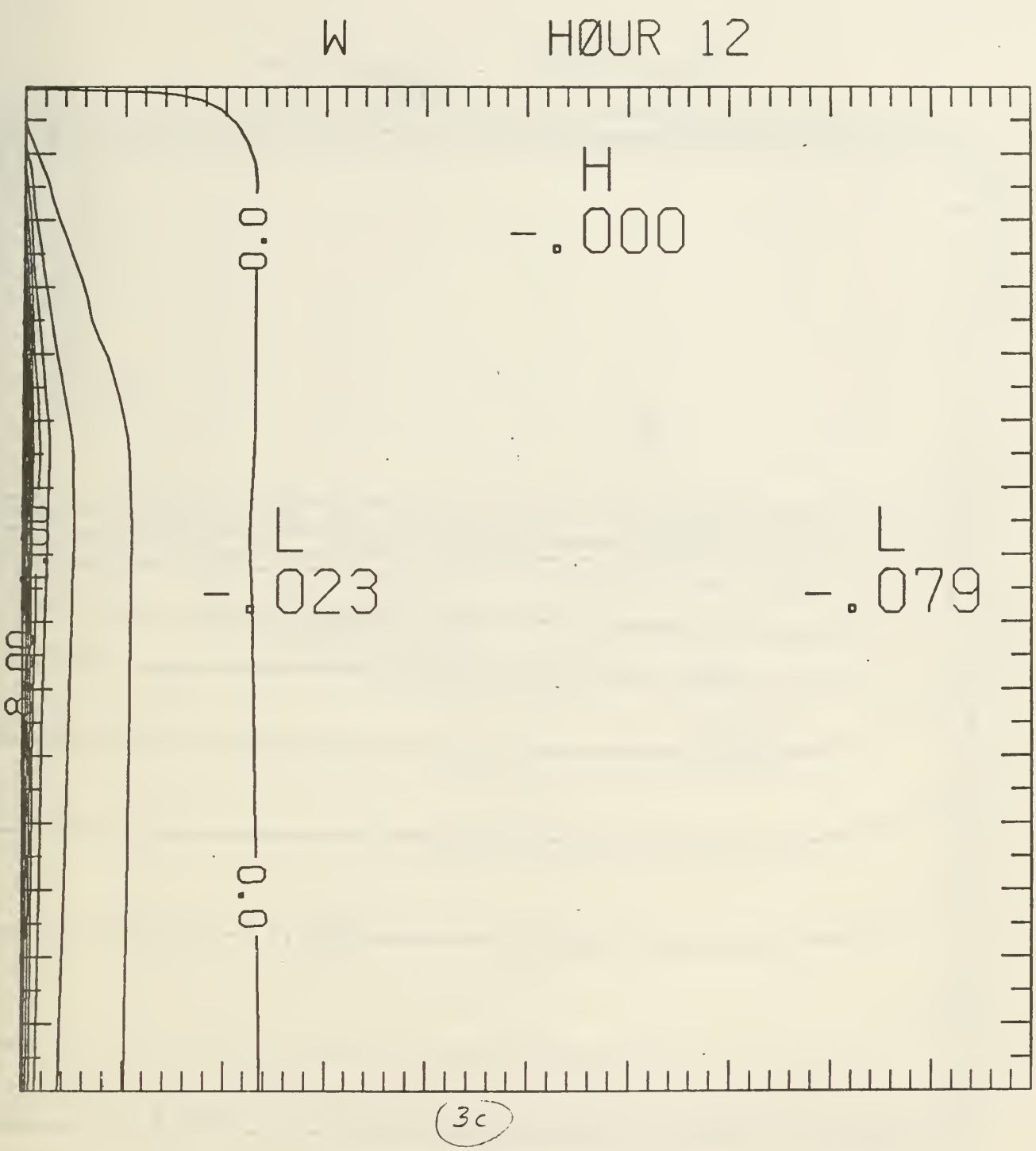
W
HØUR 12
H
-.000
L
-.023
L
-.079
0.0
0.0
8.00
(3c)

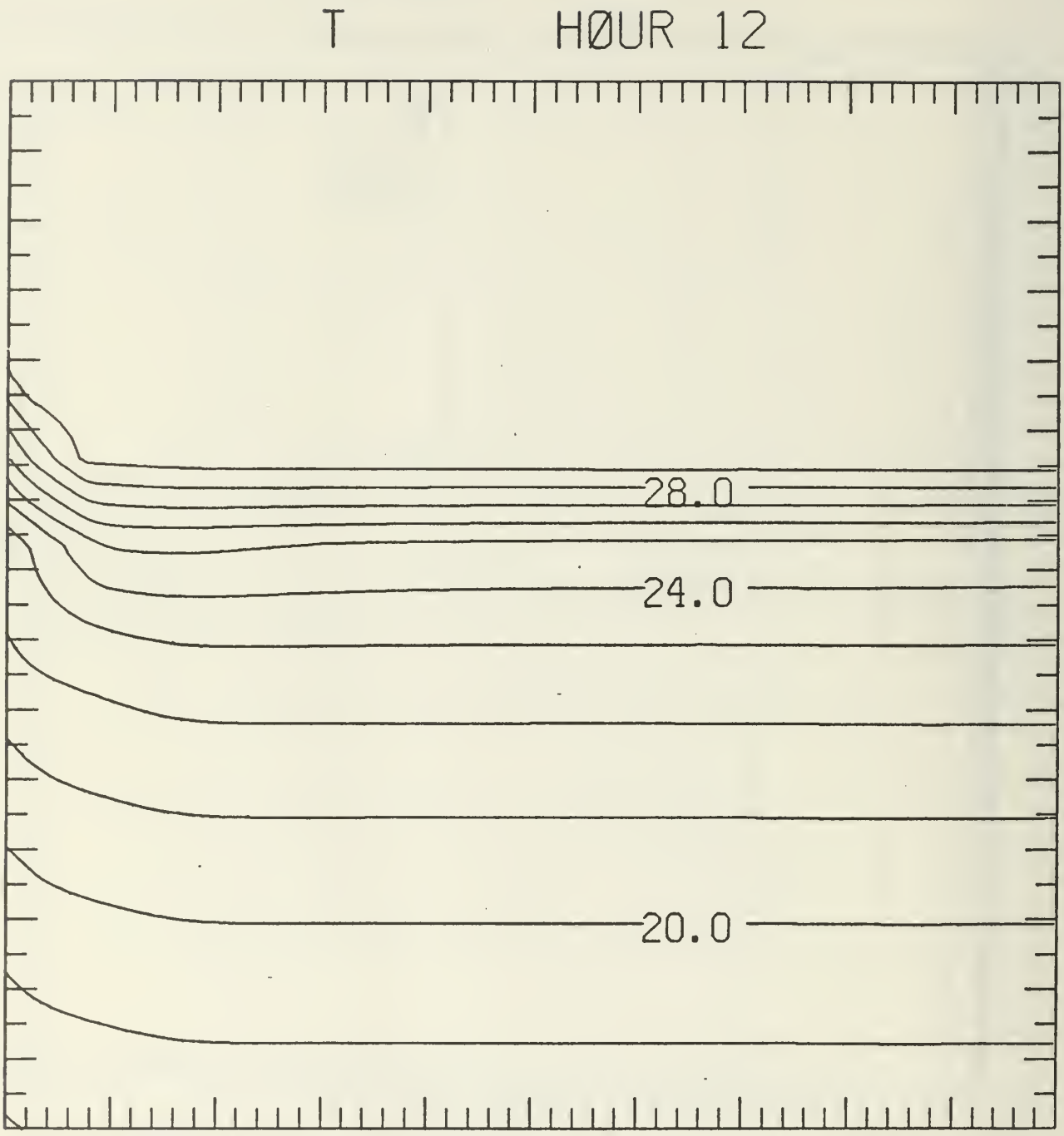

(3d)

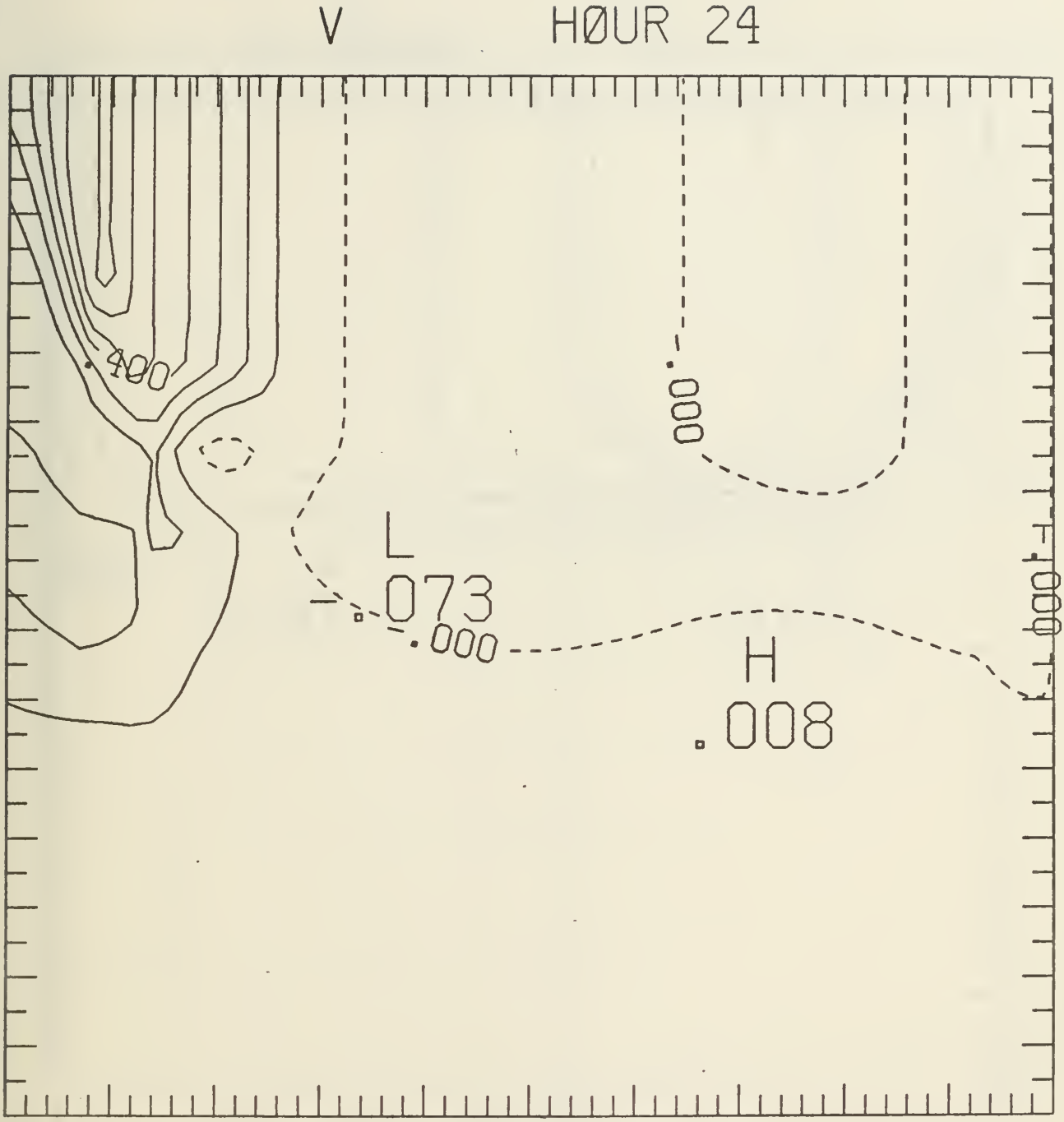

(4a)

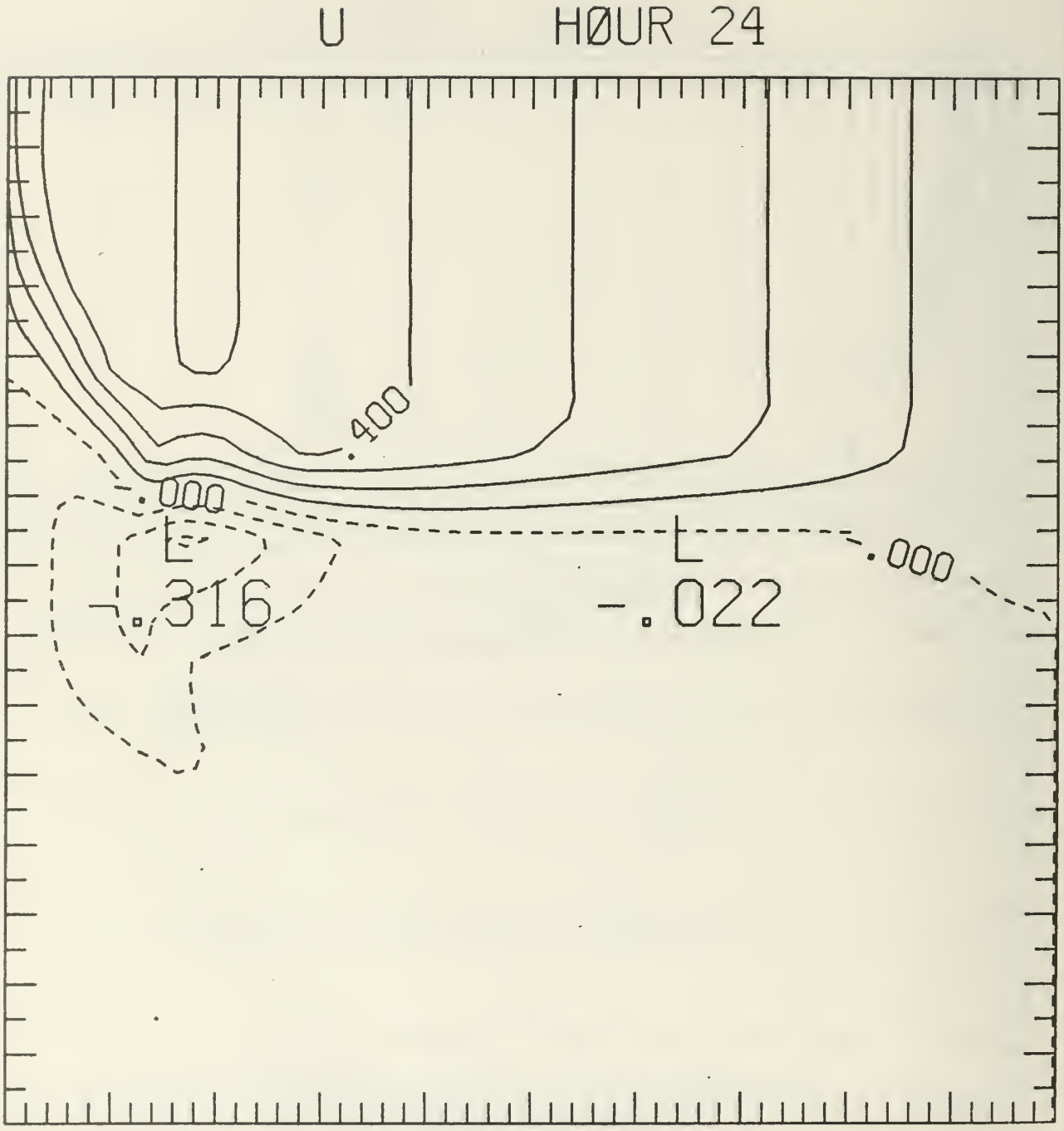

(46)

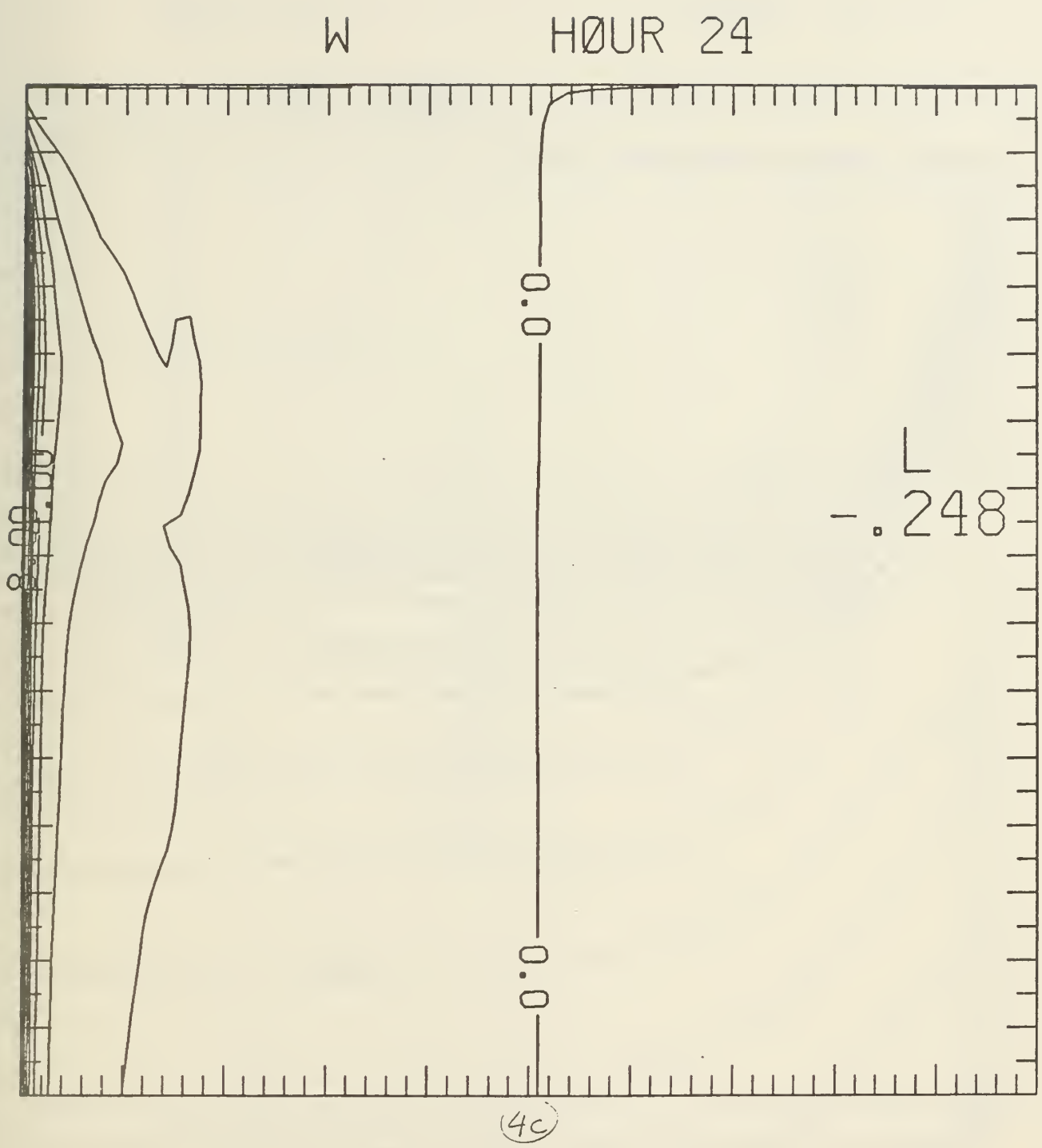
W
HØUR 24
0.0
0.0
L
-.248
(4c)

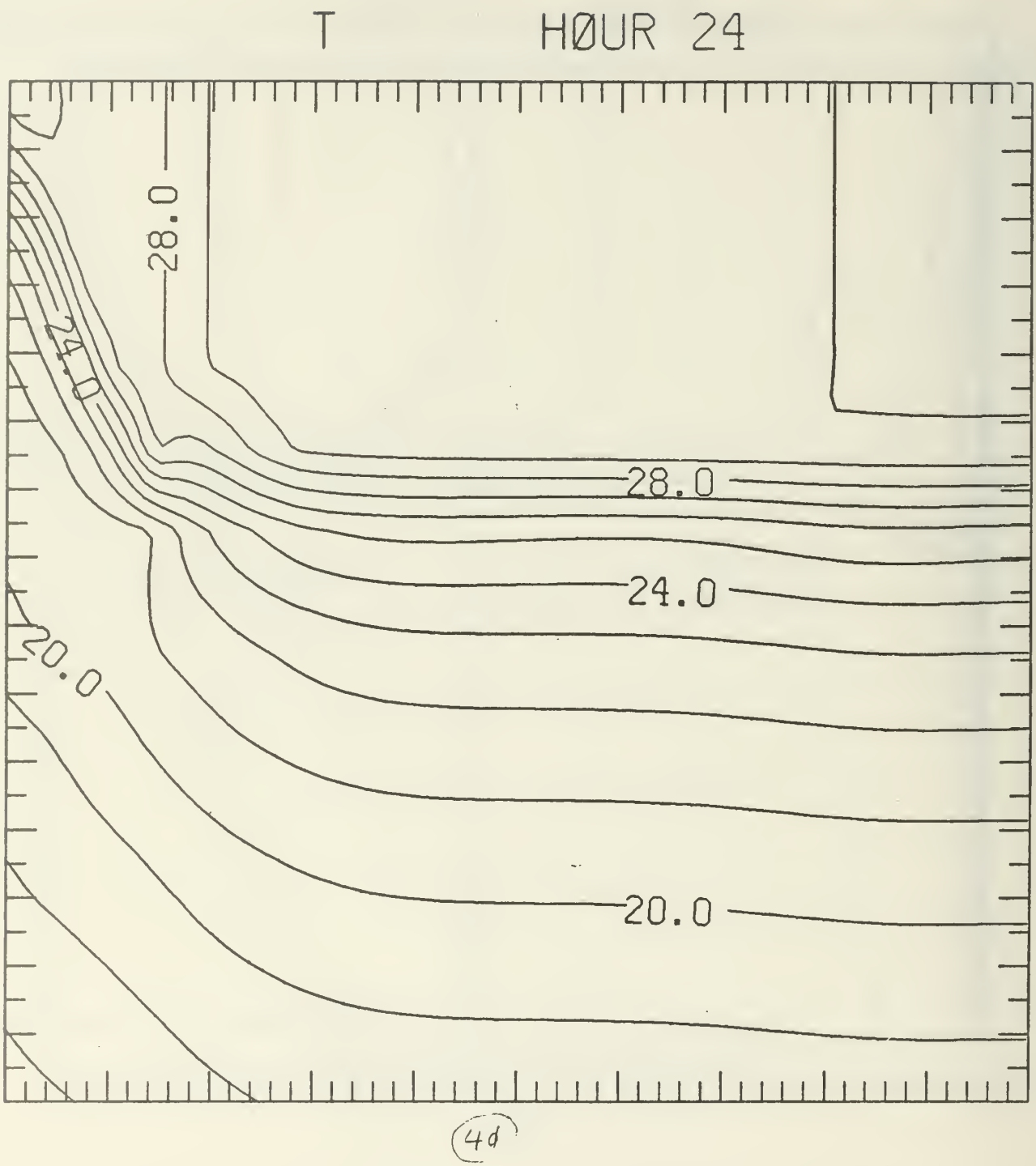
T HØUR 24
28.0
24.0
28.0
24.0
20.0
20.0
4d

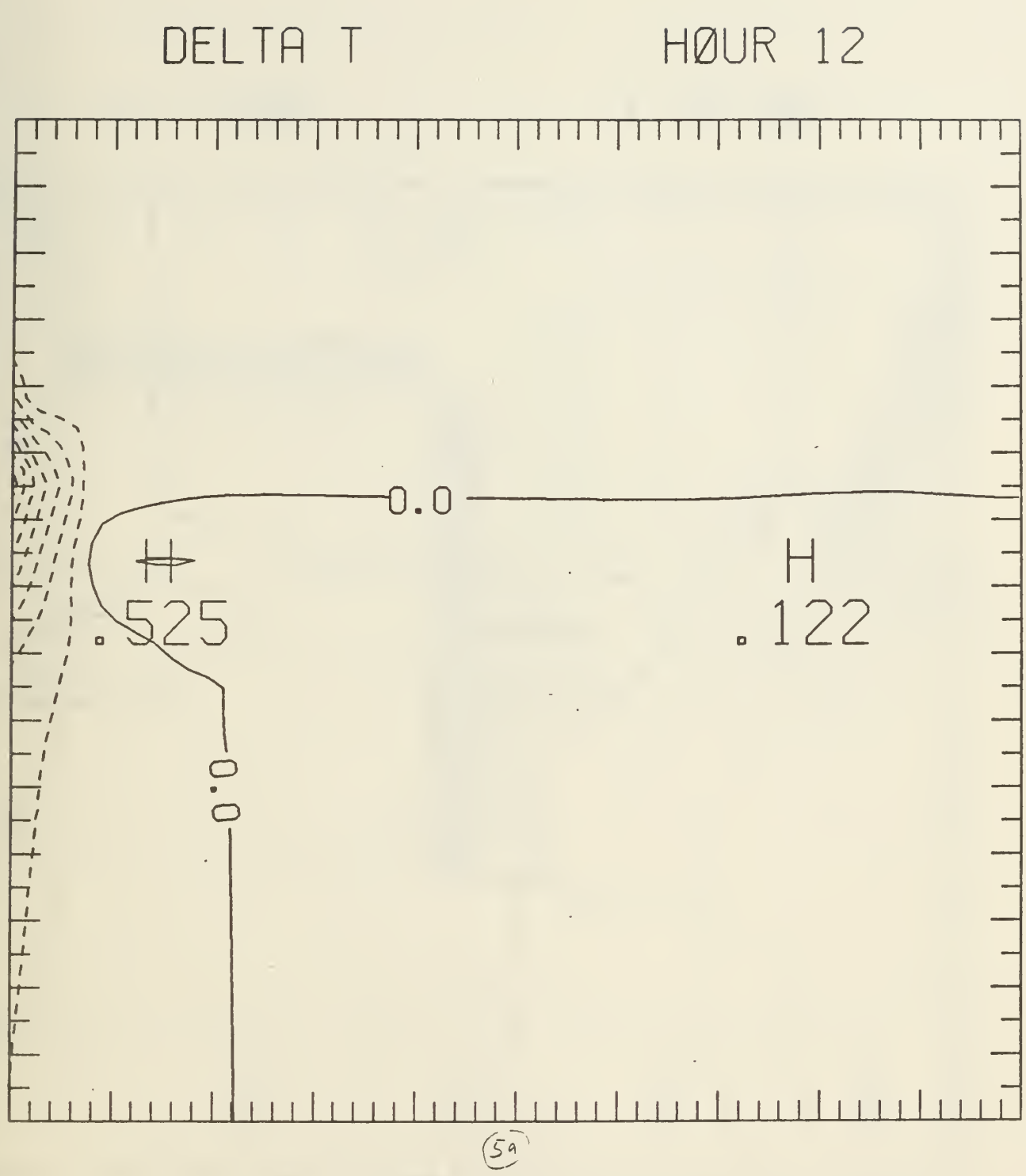
DELTA T
HØUR 12
0.0
H
.525
H
.122
0.0
(59)

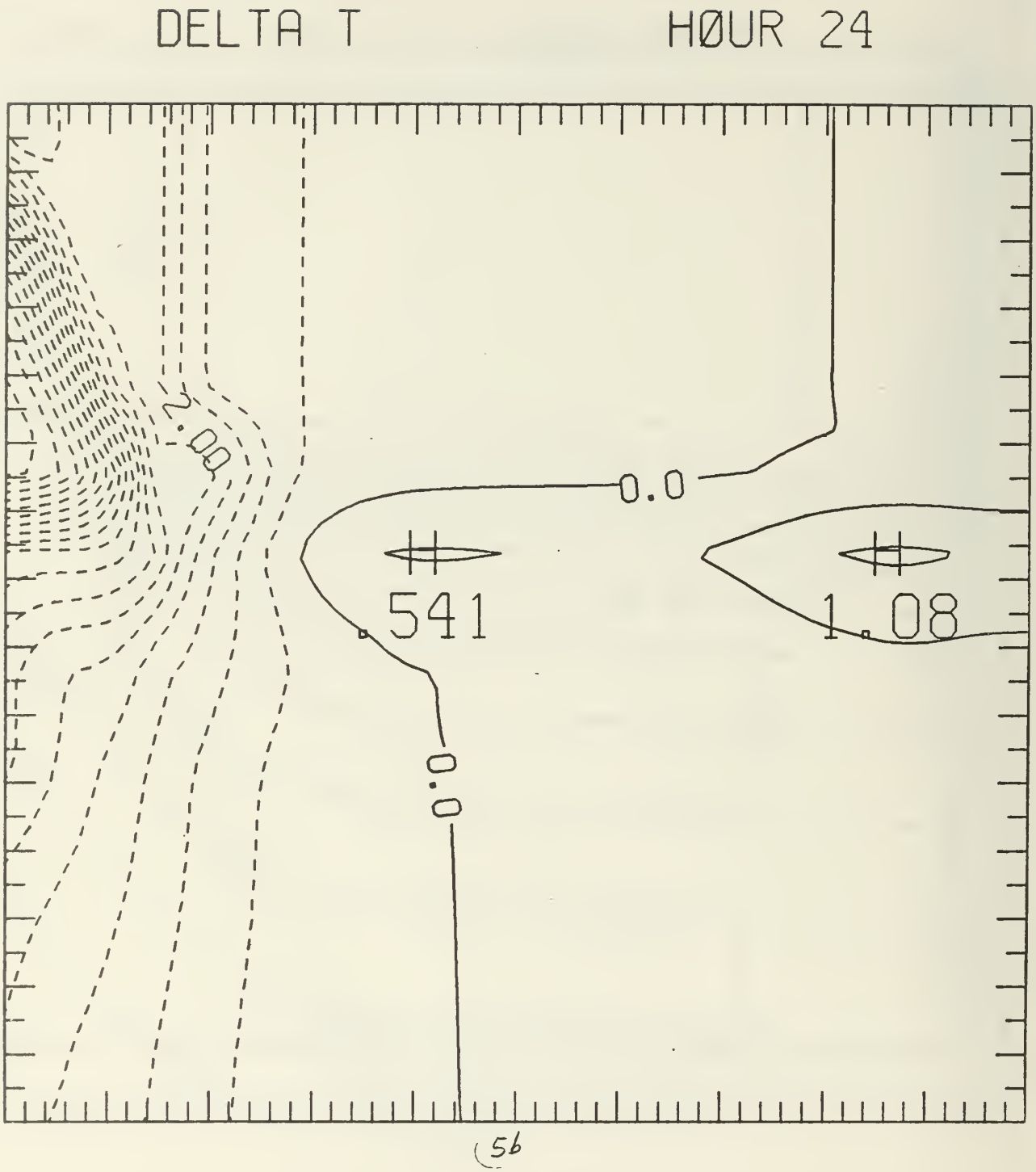
DELTA T
HØUR 24
-2.00
0.0
541
1.08
0.0
56

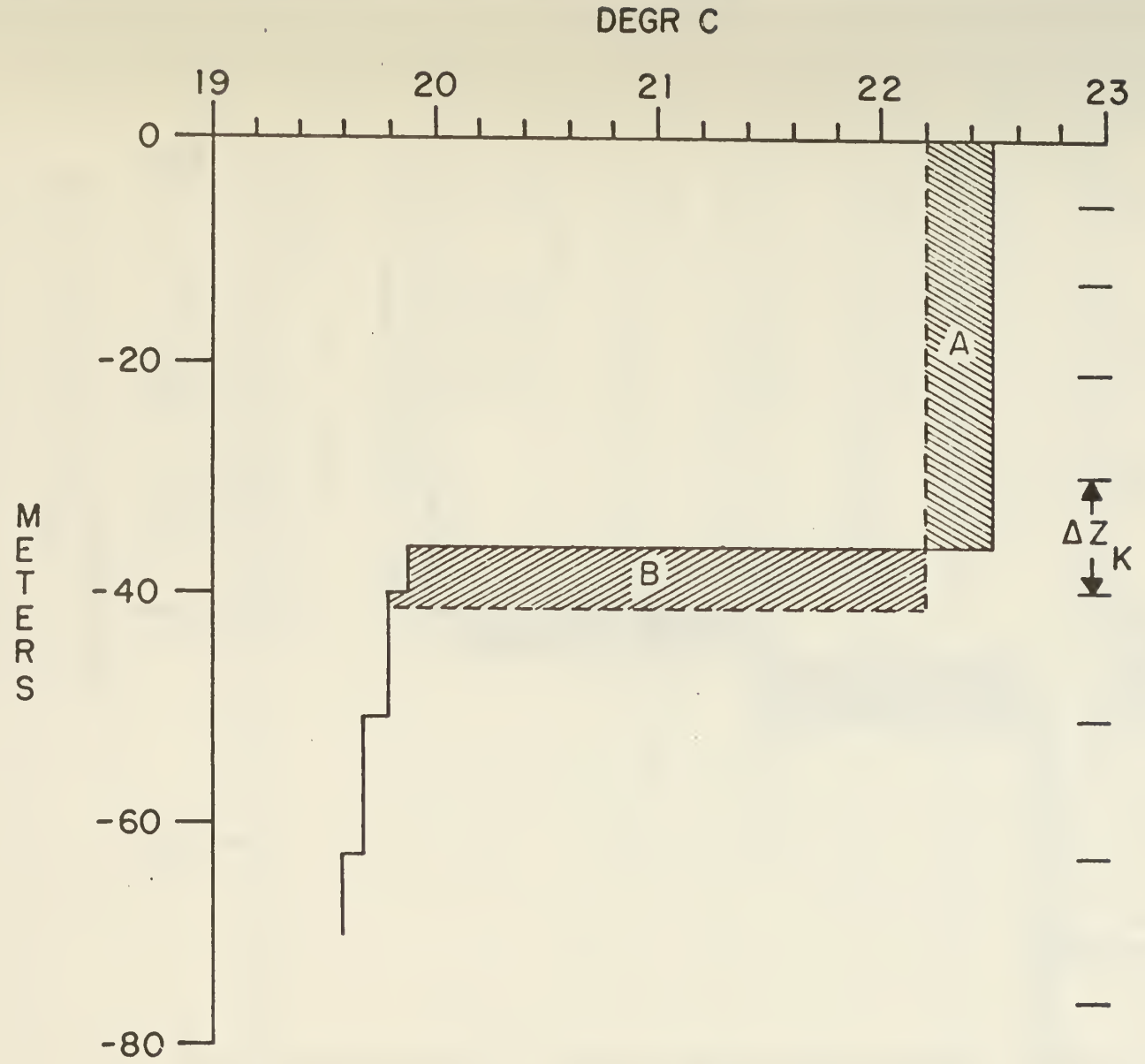

A1

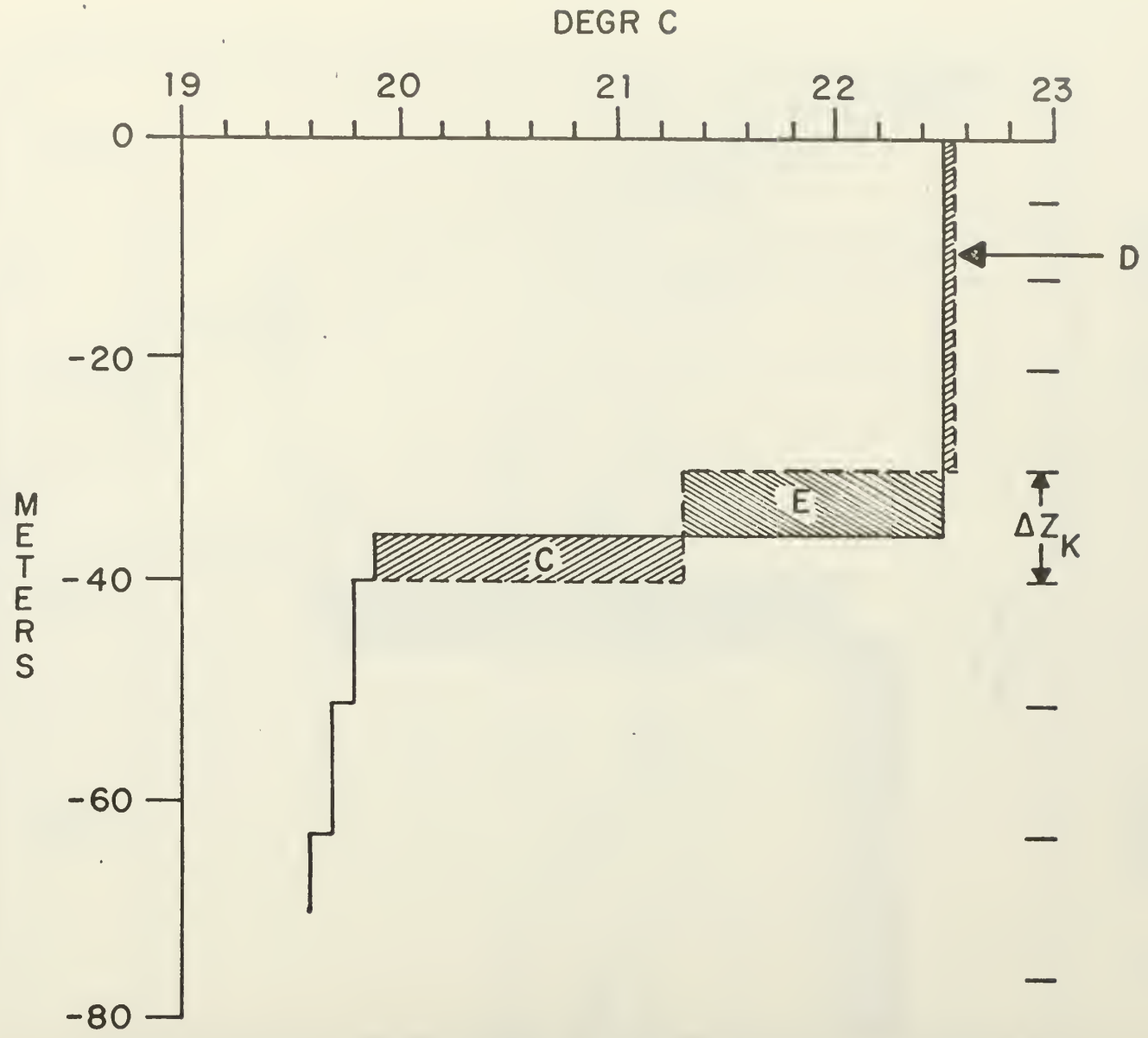
DEGR C
19
20
21
22
23
0
-20
-40
-60
-80
METERS
D
E
C
ΔZK

INITIAL DISTRIBUTION LIST

1.	Defense Technical Information Center Cameron Station Alexandria, Virginia 22314	2
2.	Library, Code 0142 Naval Postgraduate School Monterey, California 93940	2
3.	Commanding Officer (Attn: S. Piacsek) Naval Ocean Research and Development Agency NSTL Station, Mississippi 39529	1
4.	Commander Naval Oceanography Command NSTL Station, Mississippi 39529	1
5.	Commanding Officer Fleet Numerical Oceanography Center Monterey, California 93940	1
6.	Officer-in-Charge Naval Environmental Prediction Research Facility Monterey, California 93940	1
7.	Librarian Naval Environmental Prediction Research Facility Monterey, California 93940	1
8.	Commander Attn: Code 8100 Attn: Code 6000 Attn: Code 3300 Naval Oceanographic Office NSTL Station Bay St Louis, Mississippi 39522	 1 1 1
9.	Office of Naval Research Code 481 NSTL Station, Mississippi 39529	1
10.	Dean of Research, Code 012 Naval Postgraduate School Monterey, California 93940	1
11.	Prof. R. L. Elsberry, Code 63Es Naval Postgraduate School Monterey, California 93940	10
12.	Prof. R. W. Garwood, Jr., Code 68Gd Naval Postgraduate School Monterey, California 93940	10

13. Department of Meteorology, Code 63Mm — 1
Naval Postgraduate School
Monterey, California 93940

14. Prof. R. L. Haney, Code 63Hy — 10
Naval Postgraduate School
Monterey, California 93940

15. Prof. C.N.K. Mooers, Code 63Mr — 1
Naval Postgraduate School
Monterey, California 93940

16. Prof. R. J. Renard, Code 63Rd — 1
Naval Postgraduate School
Monterey, California 93940

17. Prof. A. Willmott, Code 68 — 1
Naval Postgraduate School
Monterey, California 93940

18. Mr. P. C. Gallacher, Code 63Ga — 1
Naval Postgraduate School
Monterey, California 93940

19. Department of Oceanography, Code 68 — 1
Naval Postgraduate School
Monterey, California 93940

20. Commanding Officer — 1
Naval Research Laboratory
Attn: Library, Code 2627
Washington, D.C. 20375

21. Naval Research Laboratory — 1
Code 2627
Washington, D.C. 20375

22. Office of Naval Research
Attn: Code 483 — 3
Attn: Code 460 — 1
Attn: Code 102B — 2
800 N. Quincy Street
Arlington, Virginia 22217

23. Contracting Officer — 1
ONR Code 613C: JMD
800 N. Quincy Street
Arlington, Virginia 22217

24. Deputy Under Secretary of Defense — 1
Research and Advanced Technology
Military Assistant for Environmental Science
Room 3D120
Washington, D.C. 20301

25. NODC/NOAA — 1
Code D781
Wisconsin Avenue, N.W.
Washington, D.C. 20235

26. Commanding Officer — 1
ONR Branch Officer
Attn: Dr. R. L. Lau
1030 E. Green Street
Pasadena, California 91106

27. Mr. David Adamec — 5
CEM
275 Windsor Street
Hartford, Connecticut 06120

28. Dr. David Anderson — 1
DAMTP
Silver Street
Cambridge CB3 9EW
UNITED KINGDOM

29. Dr. K. Bryan — 1
GFDL/NOAA
Princeton University
P.O. Box 308
Princeton, New Jersey 08540

30. Dr. Curtis A. Collins — 1
Program Manager
Environmental Prediction Office of IDOE
National Science Foundation
Washington, D.C. 20550

31. Dr. Claude Frankignoul — 1
Dept. of Meteorology, 54-1520
Massachusetts Institute of Technology
Cambridge, Massachusetts 02139

32. Dr. Jerry A. Galt — 1
NOAA Pacific Marine Environment Lab.
University of Washington WB-10
Seattle, Washington 98105

33. Prof. W. L. Gates, Chairman — 1
Dept. of Atmospheric Sciences
Oregon State University
Corvallis, Oregon 97331

34. Dr. Adrian E. Gill — 1
DAMTP
Silver Street
Cambridge CB3 9EW
UNITED KINGDOM

35. Dr. Lou Goodman 1
ONR Code 481
c/o NUSC, Building 101-N
Newport, Rhode Island 02840

36. Dr. David Halpern 1
NOAA/PMEL
3711 15th Avenue N.E.
Seattle, Washington 98105

37. Dr. Dale B. Haidvogel 1
Center for Earth and Planetary Sciences
Harvard University
Cambridge, Massachusetts 02138

38. Prof. Y. J. Han 1
Dept. of Atmospheric Sciences
Oregon State University
Corvallis, Oregon 97331

39. Dr. Ed Harrison 1
Dept. of Earth and Planetary Sciences
Massachusetts Institute of Technology
Cambridge, Massachusetts 02139

40. Dr. William Holland 1
NCAR
Boulder, Colorado 80302

41. Cdr. Robert G. Kirk 1
ONR Code 481
NSTL Station, Mississippi 39529

42. Dr. Jeong-Woo Kim 1
Dept. of Atmospheric Sciences
Oregon State University
Corvallis, Oregon 97331

43. Library 1
Woods Hole Oceanographic Institution
Woods Hole, Massachusetts 02543

44. Affonso da S. Mascarenhas, Jr. 1
Dept. of Meteorology & Physical Oceanography
Room 54-1711
Massachusetts Institute of Technology
Cambridge, Massachusetts 02139

45. Ekki Mittelstredt 1
Deutsches Hydrographisches Institut
Bernhard-Nocht-Strabe 78 Postfach 2 20
2000 Hamburg 4, F.R.G.

46. Dr. Bob Miller 1
Harvard University
Division of Applied Sciences
Pierce Hall
Cambridge, Massachusetts 02138

47. Dr. Peter Muller 1
Harvard University
Division of Applied Sciences
Pierce Hall
Cambridge, Massachusetts 02138

48. Dr. M. Miyake 1
Institute of Ocean Sciences
9860 W. Saanich Road
P.O. Box 5000
Sidney, B.C. V8L 4B2
CANADA

49. Dr. Mike McPhaden 1
NCAR
Boulder, Colorado 80302

50. Dr. Peter Niiler 1
School of Oceanography
Oregon State University
Corvallis, Oregon 97331

51. Dr. J. J. O'Brien 1
Meteorology Annex
930 Wildwood Drive
Florida State University
Tallahassee, Florida 32306

52. Dr. C. Paul 1
NOAA/AMOL/PLOL
15 Rickenbacker Cswy
Miami, Florida 33149

53. Prof. Allan R. Robinson 1
Harvard University
Pierce Hall
Cambridge, Massachusetts 02138

54. Dr. P. Ripa 1
CICESE
P.O. Box 4844
San Ysidro, California 92073

55. Lcdr John Roeder 1
ONR Code 481
NSTL Station, Mississippi 39529

56. Dr. Tom Sanford 1
Applied Physics Laboratory
University of Washington
1013 NE 40th Street
Seattle, Washington 98105

57. Prof. Artem S. Sarkisyan 1
Institute of Oceanol. USSR
Academy of Sciences
Moscow, USSR

58. Dr. Robert E. Stevenson 1
ONR Scientific Liaison Officer
205 Matthews Campus, UCSD
La Jolla, California 92093

59. Dr. Bert Semtner 1
NCAR
Boulder, Colorado 80302

60. Dr. Kenzo Takano 1
Rikagaku Kenkyusho
Yamato-Machi, Saitama Prefecture
JAPAN

61. Dr. Rory Thompson 1
CSIRO Division of Fisheries and Oceanography
Box 21, Cronulla, N.S.W.
AUSTRALIA, 2230

62. Dr. J. D. Thompson 1
JAYCOR
205 S. Whiting Street
Alexandria, Virginia 22304

63. Dr. Warren White 1
NORPAX A-030
Scripps Institution of Oceanography
La Jolla, California a 92093

64. Prof. Klaus Wyrtki 1
University of Hawaii Institute of Geophysics
2525 Correa Road
Honolulu, Hawaii 96822

65. Dr. W. Washington 1
NCAR
Boulder, Colorado 80302

66. Huseyin Yuce 1
Yuk. Muh. Kd. Yzb.
Sey. Hid. ve Osl. Da. Bsk. ligi
Cubuklu/Istanbul
TURKEY

DUDLEY KNOX LIBRARY - RESEARCH REPORTS
5 6853 01068159 6
U196106